Cosmic ray tracks in chondritic material with focus on silicate mineral inclusions in chromite

My Riebe

Dissertations in Geology at Lund University,
Master's thesis, no 297
(45 hp/ECTS credits)

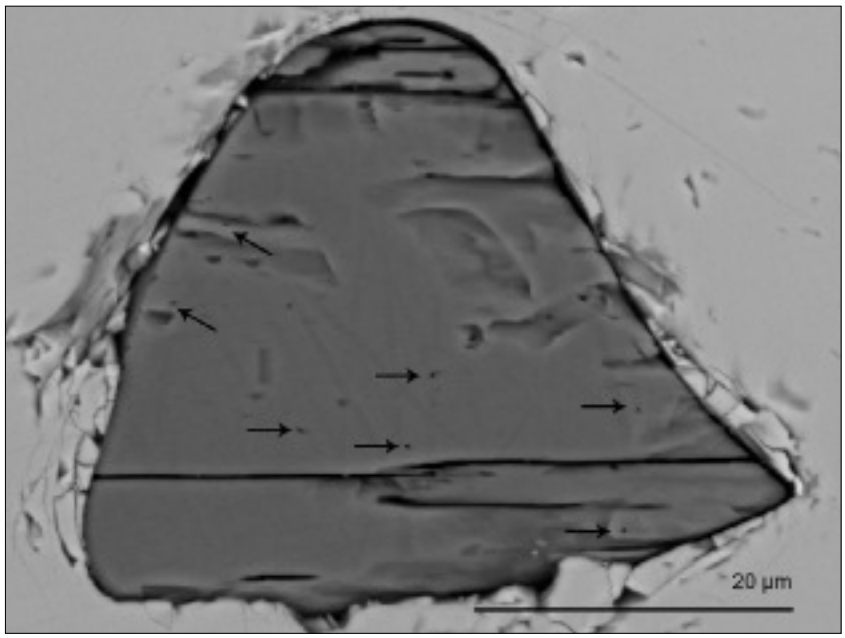

Department of Geology
Lund University
2012

Cosmic ray tracks in chondritic material with focus on silicate mineral inclusions in chromite

Master's thesis

My Riebe

Department of Geology
Lund University
2012

Contents

Cover Picture: BSE image of a pyroxene inclusion in a chromite grain from the recent meteorite Kernouvé (H6). Etch pits interpreted as galactic cosmic ray tracks are indicated with arrows.

Cosmic ray tracks in chondritic material with focus on silicate mineral inclusions in chromite

MY RIEBE

Riebe, M., 2012: Cosmic ray tracks in chondritic material with focus on silicate mineral inclusions in chromite. *Dissertations in Geology at Lund University*, No. 297, 31 pp. 45 hp (45 ECTS credits).

Abstract: It has been suggested that the cosmic ray flux varies as Earth moves relative to the spiral arms in the galaxy. However, no satisfying record over the cosmic ray flux over long time scales has been presented. This work aims to investigate the possibility to use cosmic ray tracks in silicate mineral inclusions in sediment-dispersed extraterrestrial chromite (SEC) grains as such a record. Chromite is the only common meteoritic mineral that survives on Earth for hundreds of millions of years. SEC grains, interpreted as parts of micrometeorites, have successfully been used as a proxy for the flux of chondritic material to Earth. Chromite is slightly conductive and does not record nuclear tracks. However, two-thirds of chondritic chromite grains contain inclusions of silicate minerals which do register tracks. To test etching techniques and learn more about tracks and their appearance, terrestrial apatite in thin sections of granite were etched for fission tracks, and olivine, pyroxene and merrillite in thin sections of meteorites were etched for cosmic ray tracks. Large (~40 μm) inclusions of pyroxene in chromite from a recent meteorite (Kernouvé, H6) were etched for cosmic ray tracks and such tracks were found in one of the inclusions. Hence, it is here shown that cosmic rays can penetrate chromite and register tracks in inclusions in chromite grains. Inclusions of olivine and plagioclase in four SEC grains from mid-Ordovician (470 Ma) sediments were etched for tracks; however, no tracks were found. It is concluded that it is likely that cosmic ray tracks could be found in inclusions in fossil SEC grains, but that several factors have to work together for such tracks to be found. The track studies in mineral grains in recent meteorites and inclusions of pyroxene in chromite from recent meteorites showed that inclusions have to be large (preferably ≥ 30 μm) and largely unaffected by other defects if cosmic ray tracks are to be found. Crucial is also that the inclusions have been subjected to cosmic rays for enough time to make track recording probable and that tracks were not annealed during atmospheric entry or later during their history on Earth.

Keywords: cosmic rays, cosmic ray tracks, extraterrestrial chromite, ordinary chondrites, Ordovician.

My Riebe, Department of Geology, Lund University, Sölvegatan 12, SE-223 62 Lund, Sweden. E-mail: my.riebe@gmail.com

Spår efter kosmisk strålning i material från kondriter med fokus på inklusioner av silikatmineral i kromit

MY RIEBE

Riebe, M., 2012: Spår efter kosmisk strålning i material från kondriter med fokus på inklusioner av silikatmineral i kromit. *Examensarbeten i geologi vid Lunds universitet*, Nr. 297, 31 sid. 45 hp.

Sammanfattning: Det har föreslagits att flödet av kosmiska strålningen till jorden har varierat över jordens historia, men det finns idag inget tillfredställande arkiv över kosmisk strålning över långa tidsperioder. Kromit är det enda mineralet i meteoriter som överlever långa tidsperioder (hundratals miljoner år) på jorden och friliggande extraterrestriska kromitkorn i kalksten (*sediment-dispersed extraterrestrial chromite grains*; SEC-korn) har använts som proxy för kondritinflödet till jorden. Kromit är något ledande och registrerar därför inte spår efter kosmisk strålning, dock innehåller två tredjedelar av kromitkorn från kondriter inklusioner av silikatmineral som faktiskt registrerar spår. Den här studien syftar till att undersöka huruvida det är möjligt att använda inklusioner av silikatmineral i SEC-korn som ett fossilt arkiv över kosmisk strålning. Studien är indelad i fyra delar varav de två första, fissionsspår i terrestrisk apatit samt spår efter kosmisk strålning i olivin, pyroxen och merrillit i recenta meteoriter, syftar till att testa etsningstekniker och lära mer om spårens utseende. I den andra och tredje delen av studien etsades inklusioner av silikatmineral i kromit från recenta meteoriter samt i SEC-korn. Spår av kosmisk strålning fanns i en pyroxeninneslutning i kromit från en recent meteorit, någonting som tydligt visar på att kosmisk strålning kan penetrera kromit och skapa spår i inklusioner av silikatmineral. Dock hittades inga spår i de fyra inklusioner i SEC-korn som undersöktes. Slutsatsen är att inklusioner av silikatmineral i SEC-korn potentiellt kan fungera som ett arkiv över kosmisk strålning över en geologisk tidskala, men att flera faktorer måste samverka om ett sådant arkiv ska bildas och bevaras. Studierna av spår i mineral och inklusioner av silikatmineral i kromit visade att inklusionerna måste vara relativt stora (företrädelsevis ≥ 30 μm) och i gott skick för att det ska vara möjligt att hitta spår i dem. Inklusionerna måste även ha varit utsatta för kosmisk strålning under tillräckligt lång tid för att spår ska ha registrerats, dessutom måste spåren ha undgått att brytas ner på grund av värmeutveckling i atmosfären och senare under kornens historia på jorden.

Nyckelord: kosmisk strålning, spår efter kosmisk strålning, extraterrestrisk kromit, ordinära kondriter, ordovicium

My Riebe, Institutionen för geologi, Lunds universitet, Sölvegatan 12, 223 62 Lund, Sverige. E-post: my.riebe@gmail.com

1 Introduction

It has been suggested that the flow of cosmic rays to Earth could vary as it travels relative the galactic spiral arms where most cosmic ray generating supernovas are located (e.g., Shaviv 2002; Marti and Lavielle 2009). It has further been speculated that such fluctuations in cosmic ray intensities might affect the climate on Earth and, in fact, a linkage between Earth's passage over the galaxy spiral arms and ice house ages have been made (Shaviv 2002; Shaviv and Veizer 2003). Iron meteorites have exceptionally high exposure ages and it has been proposed that different nuclide pairs in iron meteorites could be used to monitor the flux of cosmic rays over periods up to 100 Ma (Marti and Lavielle 2009). However, these ideas have still not been put into practice as one important shortcoming is that they do not cover longterm time scales, which lead to the question whether there could be any clues regarding variations in the cosmic rays flux in the geological record on Earth.

Today, about 30,000 tons of extraterrestrial matter reaches Earth every year (Peucker-Ehrenbrink and Ravizza 2000). Most of that matter is rapidly altered or weathered away. However, it is known from Ordovician fossil meteorites from the Kinnekulle area in southern Sweden that chromite ($FeCr_2O_4$), constituting 0.05-0.5 % of recent meteorites, can remain largely unaffected by alteration on Earth for hundreds of millions of years (Thorslund et al. 1984; Schmitz et al. 2001). The Ordovician limestone beds in which the fossil meteorites are found also contain exceptionally high concentrations of sediment-dispersed extraterrestrial chromite (SEC) grains. Measurements of He and Ne isotopic ratios indicate that the SEC grains arrived to Earth as parts of micrometeorites (Heck et al. 2008; Meier et al. 2010). Both the fossil meteorites and the SEC grains have been confirmed as L-chondritic and are associated with the breakup of the L-chondrite parent body 470 Ma (Schmitz et al. 2001; Schmitz et al. 2003; Schmitz and Häggström 2006; Bridges et al. 2007; Korochantseva et al. 2007). The SEC grains have proven to be useful proxies for the influx of extraterrestrial material to Earth. Could they also serve as a longtime record of the cosmic ray intensity and composition? When cosmic rays collide with crystal material they produce small defects known as cosmic ray tracks. Cosmic ray tracks are only found in insulators and semiconductors of poorer conductivity as tracks anneal if electrons can move freely in the material which is the case for a conductive material such as chromite (Fleischer et al. 1975). However, about two-thirds of chromite grains contain inclusions of silicate minerals such as pyroxene and olivine (Alwmark and Schmitz 2009; Alwmark et al. 2011), minerals which indeed do register tracks. Taken that cosmic rays can pass through chromite and register tracks in inclusions in chromite, and that such tracks can survive both atmospheric entry of micrometeorites and later sediment burial, then cosmic ray tracks in silicate mineral inclusions in SEC could serve as a record of cosmic rays over hundreds of millions of years. In addition to giving information on cosmic ray intensities based on cosmic ray track densities, cosmic ray tracks also have the potential to give clues on the composition of fossil cosmic rays, since the length of tracks correlates with the atomic number of the track producing particle (Fleischer et al. 1975).

This pilot study aims to investigate if it is possible to find cosmic ray tracks in silicate mineral inclusions in SEC grains. There are several types of nuclear tracks of which three are considered here; fission tracks, solar flare tracks and galactic cosmic ray tracks. Here cosmic ray tracks (CRT) is used as a broader term including both solar flare tracks (SFT) and galactic cosmic ray tracks (GCT). The study is divided into four parts. For the first two parts the aim was to learn etching techniques and get familiarized with nuclear tracks in general and cosmic ray tracks in particular. Firstly, terrestrial apatite was etched for fission tracks, secondly, olivine and pyroxene in chondrites were etched for cosmic ray tracks, thirdly pyroxene inclusions in chondritic chromite from recent meteorites were etched for cosmic ray tracks, and finally silicate mineral inclusions in SEC grains from mid-Ordovician, 470 Myr old, sediments were investigated for cosmic ray tracks.

2 Background

2.1 Cosmic rays

Cosmic rays are sometimes defined as charged subatomic particles including atomic nuclei, electrons (β-particles) and protons (e.g., Friedlander 2000). Here, a stricter definition is used and only atomic nuclei are considered when the term cosmic ray is used (e.g., Letessier-Selvon and Stanev 2011). In effect this more confined definition only excludes electrons from the wider definition used by for example Friedlander since protons are included in the capacity of being hydrogen nuclei. The cosmic ray beam is characterized by its elemental composition and energy spectrum.

The cosmic ray beam elemental composition is similar to solar system elemental composition (Castellina and Quispe Quispe 2009). Solar system elemental composition has been determined based on spectroscopic measurements of the solar photosphere and compositions of a special kind of pristine meteorites; CI chondrites, which have compositions that closely resemble solar composition (e.g., Asplund et al. 2005; Grevesse and Sauval 1998; Anders and Grevesse 1989; see Fig. 1). It is striking how dominating hydrogen is as the most common element in the solar system. Hydrogen nuclei, consisting of one single proton, are also most common among the cosmic rays. Second most common are helium nuclei, more commonly referred to as α-particles in

accordance with the nomenclature coined by Ernest Rutherford in the early 20th century (Friedlander 2000).

Generally, nuclei of high atomic number (Z) are less abundant in the solar system, as well as in the cosmic ray beam, than lighter nuclei (Fig. 1; Table 1). In fact, the heavier particles are extremely rare compared to hydrogen nuclei (protons); for every particle with Z>65 in the cosmic ray beam there are 3 billion protons (Friedlander 2000). Another trend in solar system elemental composition is that odd numbered elements generally are less common than even numbered elements (Fig.1). The same pattern is seen in the cosmic ray beam (Friedlander 2000).

Even though the solar system elemental composition and the cosmic ray beam composition at large are similar there is one remarkable difference; the abundance of Li, Be and B (light nuclei). The light nuclei are about 100 000 times more abundant among the cosmic rays than these elements are in the solar system (Friedlander 2000). In the solar system the light nuclei elements are relatively uncommon (Fig. 1) as an effect of the nucleosynthesis processes in stars where light nuclei are readily produced, but just as fast consumed in the formation of heavier nuclei. The extreme abundance of light nuclei among the cosmic rays is due to fragmentation of heavier nuclei during travel trough interstellar space (Castellina and Quispe Quispe 2009).

The sun is our closest star and a majority of the low energy cosmic rays in our solar system originate in the sun. The part of the sun that is visible to us is called the photosphere and has a temperature of about 6000 degrees. Outside the photosphere the corona is situated. The corona has a temperature that exceeds one million degrees. With such a high temperature some of the ionized gas reaches speeds high enough to escape the gravitational attraction of the sun. Every second roughly 300 000 tons of material, known as the solar wind, escape the sun in this way (Friedlander 2000). In spite of escaping the sun's gravitational field the solar wind particles are fairly low energy particles in a cosmic ray context. They typically travel with 0.2% the speed of light and carry an energy of about 3000 eV (electron volt; one electron volt equals the amount of kinetic energy gained by one unbound electron as it is accelerated through an electric potential difference of one volt). The solar wind particles do not produce tracks in meteoroids. However, there are events, known as solar flares, under which the sun indeed emits particles which can produce tracks in meteoritic crystals (Fleischer et al. 1975). The solar flare particles are the same type of ionized gas particles from the corona that are emitted in the solar wind, the difference lies in the energy. The energy of solar flare particles is three orders of magnitude larger (10^6 eV) than the energy of the solar wind particles and they have a speed of about 5% the speed of light (Friedlander 2000).

The cosmic ray energy spectrum ranges over kinetic energies between 10^6 and 10^{20} eV (Fig. 2; Letessier-Selvon and Stanev 2011). As seen above, the lower energies; around 10^6 eV, originate from the sun. The higher energies, in the 10^7 eV region and above, are interpreted as having a galactic, or even extragalactic, origin (Castellina and Quispe Quispe 2009). There are two shifts in the slope in the cosmic ray spectrum that are considered important in understanding the origin of cosmic rays. At around 10^{15} eV the slope steepens slightly, this is known as "the knee" and around 10^{19} eV the spectrum flattens out again to a smaller slope in the region known as "the ankle"

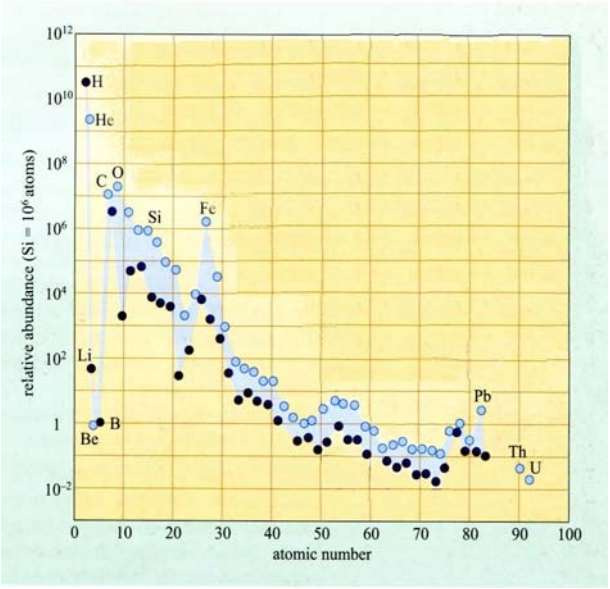

Fig. 1. Solar system elemental composition. The abundances of the elements are expressed relative Si, which is set at 10^6 atoms. Two overall trends are evident from the solar system composition. Firstly, elements with high Z are less abundant than elements with low Z. Secondly, odd numbered elements are less abundant than their even numbered neighbors. (Rogers 2007).

Table 1. Fluxes of cosmic ray particles. From Friedlander 2000.

Type of nucleus	Flux (with energies over 1.5 GeV/nucleon) Particles/m^2 *sec
H	640
He	94
Li, Be, B	1.5
C, N,O	6
F-Mn (Z=9-25)	1.0
Fe (Z=26)	0.24
Co, Ni (Z=27,28)	0.01
All nuclei with Z>28 (Ni)	0.003
All nuclei with Z>65 (Tb)	$2*10^{-7}$

(Castellina and Quispe Quispe 2009; Letessier-Selvon and Stanev 2011).

The major portion of the galactic cosmic ray beam beam is believed to be accelerated by supernova remnants (SNR; Ptuskin et al. 2010). SNR have high magnetic fields and are large and long lived enough to accelerate cosmic rays to high energies (Letessier-Selvon and Stanev 2011). Letessier-Selvon and Stanev claim that there is a general consensus in the field of cosmic ray research that particles with energies up to the knee (10^{15} eV; see Fig. 2) are accelerated in SNR and that the knee represents the maximum energy that SNR can accelerate particles to. Cosmic ray particles of energies between the knee and the ankle should then be accelerated by some unknown, efficient galactic system (Letessier-Selvon and Stanev 2011). However, there is an ongoing debate on the origin of different fractions of the cosmic ray beam, for example; Berezhko and Völk (2007) suggested that there could be an amplification of the magnetic field in SNR due to the accelerating nuclear cosmic ray component and concluded that the energy spectra up to 10^{17} eV very well could be produced in SNR and that the energy spectra up to this energy probably is dominated by SNR accelerated particles. Berezhko and Völk (2007) interpret the knee as the maximum energy that protons can be accelerated to in SNR instead of the maximum energy that SNR can accelerate any particle to (light or heavy) as the knee is more commonly interpreted (Letessier-Selvon and Stanev 2011). Cosmic ray particles with energies above the ankle (~10^{19} eV) are most likely accelerated in extragalactical systems (Berezhko and Völk 2007, Letessier-Selvon and Stanev 2011).

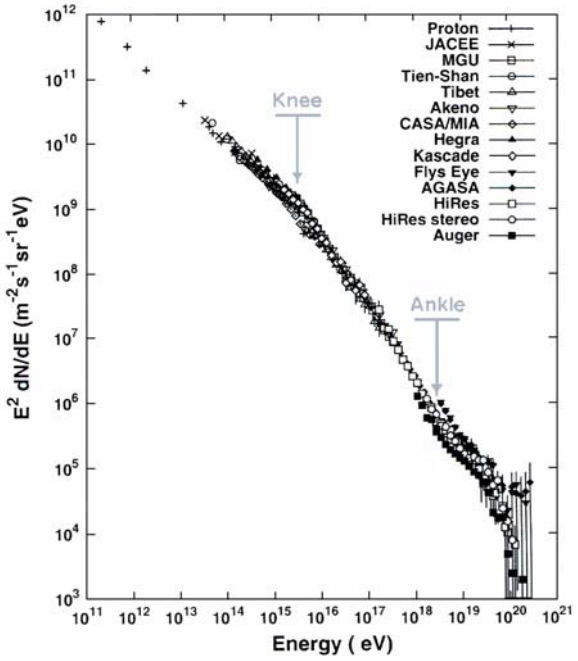

Fig. 2. Differential cosmic ray energy spectrum of energies above 10^{11}eV multiplied by E^2. In the upper right part of the image there is a legend showing the studies which have contributed to the spectrum. The energy spectrum range over kinetic energies between 10^6 and 10^{20} eV. The lowermost energies, around 10^6eV originate from the sun. There are two shifts in the slope of the energy spectrum; "the knee" at about 10^{15}eV is interpreted as the maximum energy that supernova remnants can accelerate particles (or protons) to and "the ankle" is interpreted as the maximum energy that any galactic system can accelerate particles to, i.e. particles with energies above the ankle are understood as originating from extragalactic systems. (Modified after Letessier-Selvon and Stanev 2011)

2.2 Nuclear track formation in crystal material

Upon collision with a mineral (or another inorganic solid) cosmic ray particles start losing energy through ionization. The rate at which they lose energy is dependent on their charge (Z) and velocity (v). The ionization of the material that it passes through depends on Z^2/v^2 (Friedlander 2000). The velocity (energy) of the particle dictates at what depth a track is recorded as track registration occurs when the ionization along the particle trajectory exceeds a certain critical rate of ionization loss (J_c; Fleischer et al. 1975). Fast particles have a rate of ionization loss that is lower than this value and do not register tracks until they have been slowed down sufficiently for the rate of ionization to be higher than the critical value ($J>J_c$).

Fleischer et al. (1965) developed the ion explosion spike model for nuclear track formation in crystals (Fig. 3), in which the charged particle (cosmic ray, fission fragment, etc.) creates an electrostatically unstable array of ions adjacent to its path. In this unstable region the ions eject each other from their normal sites as an effect of the Coulomb energy of the ions, creating both interstitial ions and vacant sites in the crystal lattice. After some time elastic relaxation diminishes the local stresses by spreading the strain more widely (Fig. 3c). The ion explosion spike model has later been refined (Young 1997; Rabone et al. 2008). However, it is beyond the scope of this study to in detail discuss the physics behind track formation. Of greater importance are the implications on track characteristics that follow from the formation model, these will be outlined below.

There will be a rapid decrease in track densities with depth in meteorites since high energy nuclei are less frequent than low energy nuclei (c.f. Fig. 2), leading to an angular anisotropy in the track distribution with a preferred orientation towards the closest surface (Fleischer et al. 1975). Another consequence of track formation model is that the track density at a given depth is dependent on the energy

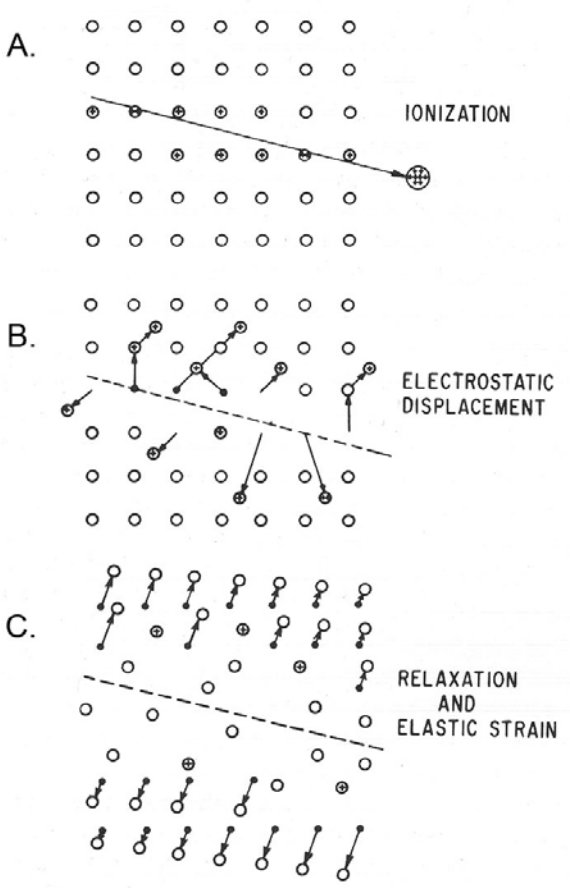

Fig. 3. The ion explosion spike model for nuclear track formation in inorganic solids. (a), the charged particle creates an electrostatically unstable array of ions along its path, (b), the ions in the unstable region get ejected from their sites, (c), local stresses are diminished by relaxation and strain is spread more widely. (Fleischer et al. 1975)

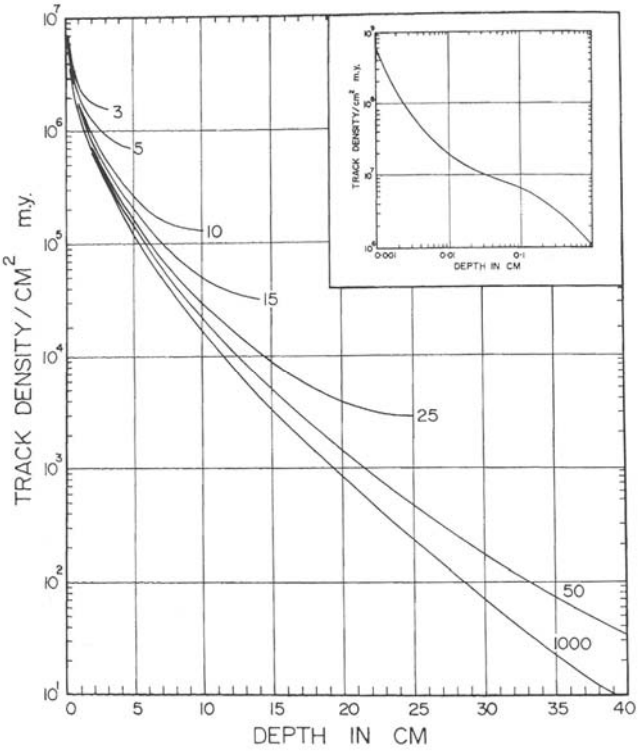

Fig. 4. Track production rate (tracks/cm^2 m.y.) as a function of depth in chondrites. Track production rates are given for chondrites with radii between 3 and 1000 cm, each represented by a curve. Track production for the outermost cm is enlarged and presented in the upper right corner. (Bhattacharya et al. 1973)

spectrum of the incident radiation, which opens up for the possibility to reconstruct the size of meteoroids prior to atmospheric entry based on track densities in different parts of meteorites (e.g., Bull and Durrani 1976). Such interpretations are possible thanks to the work by Bhattacharya et al. (1973) who estimated long-term average track production rates based on the cosmic ray charge and energy spectra and on track density observations in lunar rocks and meteorites. The work by Bhattacharya and coworkers show how track density is rapidly reduced with depth (Fig. 4). For track-producing particles with very low energies (solar flare particles) the track density changes will be visible on a micrometer scale. At higher energies, i.e. with more galactic cosmic rays, the density changes will occur on a centimeter scale (Fleischer et al. 1975).

2.3 Different types of tracks

Three different types of nuclear tracks are of interest to this study; fission tracks (FT), galactic cosmic ray tracks (GCT) and solar flare tracks (SFT). Their characteristics are described below.

Apatite in terrestrial samples is used for low temperature FT dating. In terrestrial apatite FT are produced by spontaneous fisson of ^{238}U. They are formed continuously through time but become annealed at elevated temperatures. For apatite the annealing temperature is around 100°C (Wagner 1968). The track density corresponds to the time that has passed since the grain cooled into the partial annealing zone. FT always have an isotropic distribution due to the random distribution of fissionable elements. Spontaneous fission tracks are also present in meteoritic phosphate minerals, such as Cl-apatite and merrillite, which incorporate ^{238}U and the now extinct isotope ^{244}Pu in the crystal lattice. Cosmic rays may induce fission of heavy atoms in minerals other than phosphate minerals. Induced fission can be produced directly by collision of high-energy cosmic rays with heavy nuclei or indirectly by

collision of secondary neutrons with heavy nuclei (Fleischer et al. 1975). Secondary neutrons are produced when cosmic rays collide with "ordinary" nuclei in the minerals. Indirect induced fission by cosmic ray produced neutrons is more common than direct induced fission. Contribution of tracks from fission induced by cosmic ray protons and secondary neutrons is always minor in chondrites (Crozaz et al. 1989).

GCT tracks are formed when cosmic ray particles of galactic origin are slowed down in meteoritical crystals and form tracks. Light elements do not form tracks in crystal material. The nuclei that form tracks are conventionally divided into two groups; very heavy nuclei (VH) comprised of nuclei $18 \leq Z \leq 30$ and very very heavy nuclei (VVH) with $Z \geq 31$ (Fleischer et al. 1975). Solar flare particles have lower energies than galactic cosmic ray particles. Hence, they cannot penetrate as deep into the crystal and SFT are characterized by a very steep gradient (μm scale; Fleischer et al. 1975; see Fig. 5). SFT have been studied in lunar rocks (e.g., Crozaz et al. 1970) and regolith breccias (e.g., Metzler 2004). SFT acquired during the transit of meteorites to Earth are destroyed as an effect of melting and ablation upon atmospheric entry (Battacharya et al. 1973).

2.4 When in the history of a meteorite are tracks formed?

Essentially, cosmic ray tracks form whenever minerals that can record such tracks are exposed to cosmic rays. It has been suggested that the earliest tracks formed before accretion in the gas-dust protoplanetary nebula, in the very beginning of the solar system history, a setting in which CRT could be produced by locally accelerated ions of iron-group elements in the solar wind (Alexeev et al. 2008). After accretion, CRT can be produced in material that is situated in, or close to, the parent body regolith (Alexeev et al. 2008; Metzler 2004; Caffee et al. 1987). The third stage of CRT production occurs between the separation of the meteoroid from the parent body and the entrance of the meteorite into the Earth atmosphere (Perron 1993). In this stage the amount of CRT recorded is dependent on the depth of the crystal relative the surface of the meteoroid (Battacharya et al. 1973).

2.5 Annealing processes and temperatures

Thermally induced diffusion allows for annealing of nuclear tracks (Reiners and Branton 2006). Understanding the parameters controlling partial and complete annealing of FT in terrestrial apatite is essential to FT chronologists and considerable effort has been put into understanding FT annealing (e.g., Ketcham et al. 1999). Fission track annealing in apatite is of minor interest to this study. Of greater importance is annealing of GRT and SFT, which are processes less well understood than FT annealing. Two annealing processes are of greatest importance when studying cosmic ray tracks in silicate mineral inclusions in SEC grains. Firstly, the annealing of tracks in micrometeorites upon atmospheric entry. Secondly, the possible annealing during sediment burial.

Atmospheric entry heats up all particles to some extent, but not in equal amounts (Love and Brownlee 1991). When modeling melting in micrometeorites Love and Brownlee (1991) found that melting is dependent on size and atmospheric entry angle and that there is a window of entry for which melting does not occur in micrometeorites. For micrometeorites with velocities typical for chondritic micrometeorites (~12 km/s) particles less than 100 μm in diameter survive melting whereas most of the larger particles melt. For particles larger than 100 μm it is only the ones which enter the atmosphere with very high angles that make it down to the Earth surface without melting (see Fig. 6).

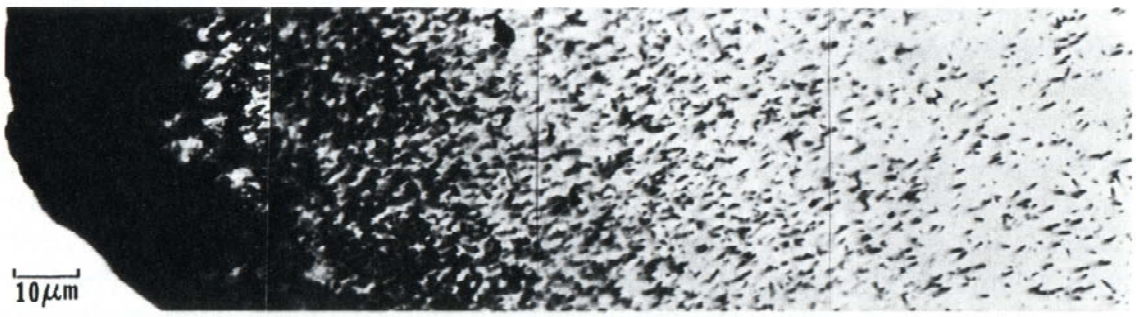

Fig. 5. Solar flare tracks in a lunar (Apollo 17) boulder. Solar flare tracks are characterized by steep track density gradients. (Fleischer et al. 1975)

Empirical evidence that tracks can survive the atmospheric entrance without complete annealing comes from solar flare tracks in Interplanetary Dust Particles (IDPs) collected from the stratosphere (Bradley et al. 1984). Bradley and collaborators also found that the IDPs with tracks had high S/Si ratios which further support low heating since S is a volatile element and would escape upon significant heating. However, out of five investigated IDPs, only two were found to contain solar flare tracks, indicating that some IDPs might have been heated above annealing temperatures (Bradley et al. 1984).

Presently, no studies on cosmic ray track annealing during prolonged periods of elevated temperature and pressure have been presented. However, a few studies can give clues on the behavior of tracks during sediment burial (Wagner 1968; Price et al. 1973; Fleischer et al. 1975; James and Durrani 1986). Annealing effects of hydrostatic pressure are typically negligible compared to temperature in normal geothermal gradients on Earth (Fleischer et al. 1975 and references therein). Tracks in olivine, pyroxene and feldspars can be partly annealed, i.e. shortened, if subjected to lunar surface temperatures (~130°C) for a million years (Price et al. 1973). However, they would not be completely annealed under these circumstances. Annealing experiments of fission tracks produced by a ^{252}Cf source resulted in complete annealing of tracks in olivine at temperatures between 490 and 550°C during one hour annealing, the higher temperatures being valid for more Fe-rich olivine and the lower temperatures for Mg-rich olivine (James and Durrani 1986). Complete annealing of fission tracks in terrestrial apatite occurs around 100 °C on long time scales (Wagner 1968). If all these facts are considered it is not likely that cosmic ray tracks would anneal completely at temperatures less than 100°C.

2.6 Methods for track studies

The tracks after heavily charged particles in crystals consist of a disorder in the structure of the material. This makes the tracks more sensitive for chemical etching than the surrounding undamaged material (Fleischer et al. 1965). Tracks that intersect the surface of the crystal will therefore be etched at a higher rate than the general etching rate of the material, allowing development of tracks that are visible in optical microscopy. Tracks that do not intersect the surface, or another defect that can channel the etchant to a confined track, will not be developed (Fleischer et al. 1965). Track etching on a given substance is affected by the etchant, temperature, concentration and the orientation of the attacked surface (Fleischer at al. 1965). Different etchants are suitable for different minerals.

In the early 70's a few labs were working with cosmic ray track studies. These labs had developed and used different etching techniques, different mounting techniques (grain mounts, thin sections, thick sections) and different imaging techniques. Some labs used SEM imaging, others optical microscopy with a variety of methods for coloring of tracks and yet others used replicas of tracks (Yuhas et al. 1972). This led to the question of how well track density measurements from different labs agreed with each other. In Yuhas et al. (1972) five cosmic ray track laboratories (Washington University St Louis, Missouri; Musee d'Histoire Naturelle Paris, France; University of California, Berkeley, California; General Electric Laboratory, Schenectady, New York; Tata Institute, Bombay, India) did track counts on the same samples, and it was found that the track density agreement was within 20% for the majority of the samples. The statistical uncertainties were typically 10% but uncertainties as high as 30% were estimated for the solar flare track regions, i.e. the outermost 1 mm (Yuhas et al. 1972).

In the early days of nuclear track studies transmission electron microscopy (TEM), which allows for studies of un-etched tracks, was used to study the basic properties of tracks (e.g., Price and Walker 1962a; Price and Walker 1962b). Fission tracks typically have a width of about 100 Å in TEM (Price and Walker 1962b). However, this width is interpreted as the long range strain of the track and the basic damaged region is estimated to around 60 Å (Price and Walker 1962a; Price and Walker 1962b; Fleischer et al. 1975). Samples cannot be more than a few hundreds of nanometers thick in order to be investigated with TEM, leading to extensive sample preparation. The field of view is relatively small and this technique is subsequently most useful for small samples and samples with high track densities.

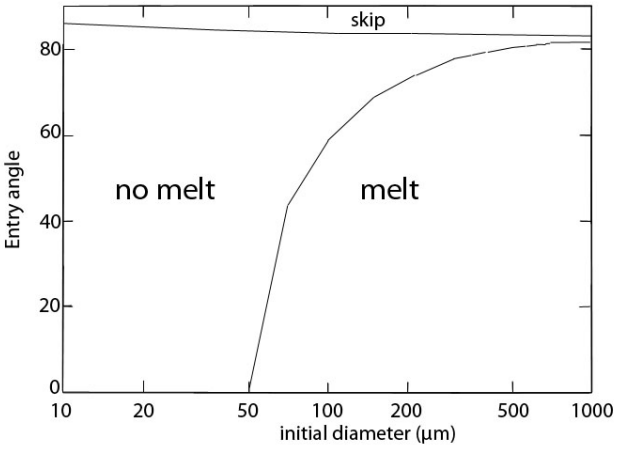

Fig. 6. Window of atmospheric entry where melting does not occur in micometeorites with a velocity of 12 km/s. For very high entry angles micrometeorites will not fall down on Earth, but "skip" back into space. (modified after Love and Brownlee 1991)

2.7 Mineralogy of ordinary chondrites and implications for track formation/ visualization

2.7.1 Classification of ordinary chondrites

Meteorites are classified into two main types; differentiated and non-differentiated meteorites. The differentiated meteorites originate from bodies which have been melted and differentiated into a high density iron core with lower density material surrounding it. The non-differentiated meteorites are often referred to as chondrites. More than 80% of the modern falls of meteorites are chondrites (Bevan et al. 1998 and references therein). Chondrites have maintained a pristine morphology and chemical composition since their formation in the early days of the solar system. Most chondrites have a characteristic chondrulic texture, consisting of sub spherical objects in the size range of tens of micrometers to a few millimeters. Chondrules are believed to once have been melted droplets in a low gravity field before they accreted and formed the parent bodies which chondritic meteorites originate from (Perron and Zanda 2005).

Chondrites are divided into three major classes based on mineralogy, bulk chemistry and oxidation state; ordinary chondrites, carbonaceous chondrites and enstatite chondrites (Fig. 7), of which ordinary chondrites are of most interest here. The ordinary chondrites are most common among meteorites; they comprise about 94% of all modern chondrite falls and finds (Bevan et al. 1998 and references therein). They have an intermediate oxidation state, somewhere between carbonaceous and enstatite chondrites, with some Fe-Ni metal. Ordinary chondrites are divided into three groups based on their chemical composition; H, L and LL (Fig. 7).

Van Schmus and Wood (1967) introduced a classification based on petrology to complement the chemical classification. The petrologic type classification is meant to be a complement to the other classification and mainly describes the degree and character of alteration of the chondrites. Van Schmus and Wood introduced 6 petrologic types. Types 1 and 2 reflect different degrees of aqueous alteration and are only found among the carbonaceous chondrites (Perron and Zanda 2005). Type 3 is the least altered of the petrologic types and types 4 to 6 represent increasing degree of thermal metamorphism. All ordinary chondrites are of petrologic types 3-6 (Fig. 7).

The classification of ordinary chondrites into petrologic types is important here mainly since it describes composition of minerals and grain size, which increase with petrologic type. In Van Schmus and Wood's original description of the types there is a gradual increase in equilibration in olivine and pyroxene. In types 5 and 6 the olivine and the pyroxene composition is uniform over the meteorite. With increasing petrologic type there is a development of secondary feldspar. It is well developed as interstitial grains in type 6 chondrites, whereas in types 4 and 5 the feldspar exist as microcrystalline aggregates and it is completely absent in type 3. Chondrules are very sharply defined in type 3 chondrites, but become less and less pronounced with increased petrologic type (Van Schmus and Wood 1967).

2.7.2 Silicate mineral inclusions in chondritic chromite as cosmic ray archives

Alwmark and Schmitz (2009) reported that silicate mineral inclusions are present in chromite from recent chondritic meteorites, fossil chondrites and SEC grains. About 2/3 of all chromite grains from recent chondrites contain inclusions of other minerals (Alwmark et al. 2011). The most common minerals in chromite inclusions are olivine and pyroxene, followed by merrillite and plagioclase. Inclusions of Cl-apatite, rutile and trolite are also present in chromite, even though they are much less frequent and smaller in size than the other minerals (Alwmark and Schmitz 2009). With the aid of synchrotron radiation X-ray tomography microscopy it has now been showed that inclusions as large as ~100 μm are present in chromite grains from recent chondrites (Alwmark et al. 2011). Alwmark and others also found that the size of inclusions varies with petrologic type. Type 6 chondrites had the largest inclusions with an average inclusion size more than 20 times larger than inclusions in chromite from types 4 and 5 chondrites.

Class	Carbonaceous chondrites							Ordinary chondrites			Enstatite chondrites	
Group	CI	CM	CR	CO	CV	CK	CH	H	L	LL	EH	EL
Petrologic type	1	1-2	1-3	3	2-3	3-6	2	3-6	3-6	3-6	3-6	3-6

Fig.7. Classification of chondrites. Chondrites are divided into three classes. Carbonaceous chondrites, ordinary chondrites and enstatite chondrites of which carbonaceous chondrites are the most oxidized and enstatite chondrites are the most reduced. Classes are further subdivided into groups. Petrologic type describes the amount and character of alteration. Petrologic types 1 and 2 describe aqueous alteration, in type 3 the least altered chondrites are found and types 4-6 represents increasing thermal metamorphism. (after Brearley & Jones 1998; Hutchison 2004)

3 Methods

3.1 Fission tracks in terrestrial apatite

For fission track studies thin sections of Siljan granite belonging to the Trans- Scandinavian Igneous Belt (TIB) were used. The Siljan granite had been sampled by Holm et al. (2011). Holm and collaborators sampled the area to investigate the distribution of shock-metamorphic features across the Siljan impact structure. Here, only samples that were found not to be affected by the impact have been used. The thin sections were searched for apatite using optical microscopy. Apatite grains were documented by optical photography in transmitted and reflected light using a 100x dry objective and Infinity 1 camera. The grains were also documented with backscattered electron images (BSE) in variable pressure scanning electron microscope (VPSEM; Hitachi S-3400N).

For track studies in phosphate minerals in extraterrestrial samples a few different methods have been used (e.g., Pellas and Strozer 1981; Crozaz et al. 1989; Perron 1993). However, etching conditions for fission track dating in terrestrial apatite are standardized to 20 s at room temperature in 5 M HNO_3 (e.g., Gleadow et al. 1986; Hurford et al. 1999; Grist 2004), and this etching method was used following careful documentation of the initial state of the grains. After 20 s the thin sections were immediately put in a large beaker of tap water to prevent further etching. The thin sections were then rinsed under running water and with distilled water. Water in the tracks can make them difficult to detect in optical microscopy, and to dry out the tracks properly the thin sections were rinsed with methanol, dabbed with a lint free cloth soaked in methanol, rinsed with methanol again and finally dried with a dry lint free cloth to prevent any impurities from the methanol from remaining on the sections (see also Grist 2004 for description on FT dating methodology). The apatite grains were then documented again using the same imaging techniques.

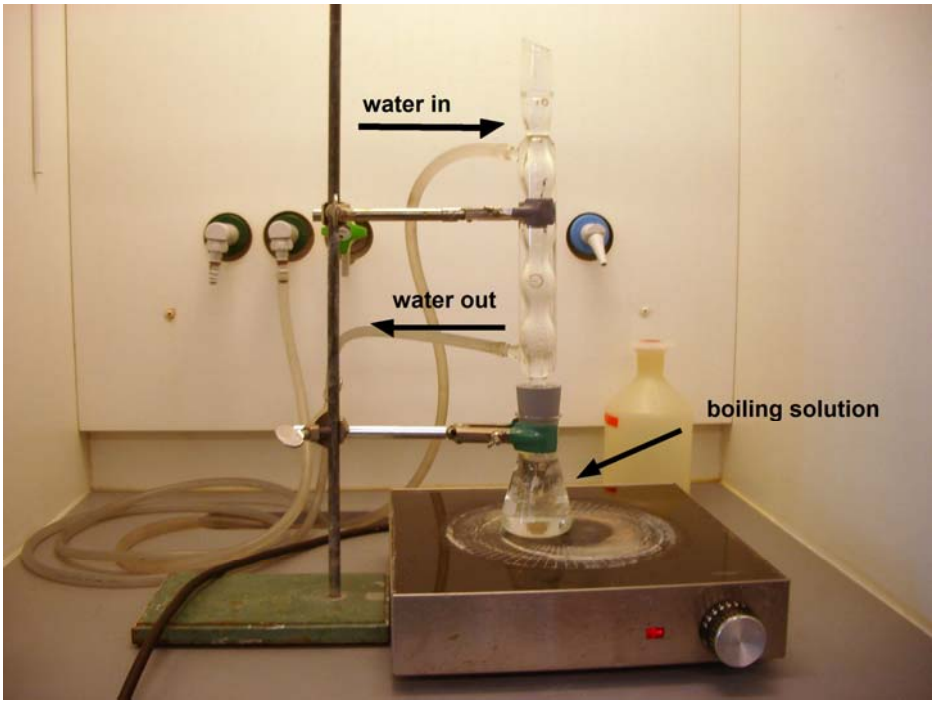

Fig.8. The reflux system described by Lal et al. (1968). The boiling solution is kept at constant temperature and concentration by collecting the water vapor in a water cooled jacket. All experiments were performed in fume cupboards.

Table 2. The samples used for CRT studies in recent meteorites.

Meteorite	Sample	Etching conditions	Etched mineral
Ozona (H6)	Ozona 1	4h WN*	Olivine
	Ozona 2	4h WN	Olivine
	Ozona 3	2h WN	Olivine
	Ozona 4	5min NaOH-solution¤	Pyroxene
Holbrook (L/LL 6)	Holbrook 1	4h WN	Olivine

*Krishnaswami et al. 1971
¤Lal et al. 1968

3.2 Cosmic ray tracks in olivine, pyroxene, and merrillite from recent meteorites

For studies of cosmic ray tracks in minerals of recent chondrites four thin sections of Ozona (H6) and one thin section of Holbrook (L/LL6) were used (Table 2). The thin sections were searched for either olivine (Ozona 1-3 and Holbrook 1) or pyroxene (Ozona 4) and selected grains were documented using BSE imaging in VPSEM and high magnification optical microscopy. Ozona 1-3 and Holbrook 1 were etched in boiling "WN-solution", described by Krishnaswami et al. (1971). The WN etchant is prepared by successive mixing of 1 g oxalic acid, 1 ml orthophosphoric acid (85 %) and 40 g disodium salt of EDTA in 100 ml distilled water, with pH adjusted to 8.0 ± 0.3 by adding NaOH pellets (Krishnaswami et al. 1971). The samples were etched in the boiling solution for two or four hours, see Table 2. To maintain a constant concentration the reflux system described by Lal et al. (1968) was used (Fig. 8). In the reflux system a water cooled jacket is attached to the top of the beaker. The vapor is cooled and condensed when it passes through the jacket and water drips back down into the solution. This way the solution is kept at constant concentration and temperature in spite of boiling for hours. The samples were washed in tap water, distilled water and methanol as described for FT in 3.1. and the outcomes of the etchings were studied using BSE and optical microscopy. Etch pit densities for individual olivine grains in one chondrule in Ozona 3 were counted using BSE images with 900x magnification. The areas of the grains in which the etch pits were counted were measured using Quartz PCI.

For etching of tracks in pyroxene an acid etch of HF, H_2SO_4 and H_2O as well as a base etch NaOH and H_2O have been used as standard techniques (Price et al. 1973). Price et al. (1973) found that a base etch is to prefer over acid etch since the etch rate is more constant, and also the base etchant develops tracks with lower ionization rate. Here, the NaOH solution described by Lal et al. (1968) was used to etch tracks in pyroxene in Ozona 4. Lal and collaborators suggested a boiling solution of 6 g NaOH in 4 ml water, with concentration and etching temperature secured by the reflux system, for pyroxenes. They found that etching times for proper development of tracks increase with increased Fe content in the pyroxene and suggested 30-40 min for enstatite $MgSiO_3$, 35-50 min for the bronzite $(Mg,Fe)SiO_3$ and 45-55 min for the more iron rich hypersthene $(Mg,Fe)SiO_3$. Ozona 4 was etched for five min (~1/8) of normal etching time for proper development of tracks) in a boiling solution of 6 g NaOH in 4 ml water (Lal et al. 1968). The sample was washed in tap water, distilled water and methanol following etching (see 3.1, Grist 2004). The thin section was then studied and photographed using SEM and optical microscopy.

3.3 Cosmic ray tracks in silicate mineral inclusions in recent chondritic chromite

Two large Ca-poor pyroxene inclusions in chromite grains from Kernouvé (H6) were searched for cosmic ray tracks, Px incl. 1 and Px incl. 2. The two chromite grains were studied by Alwmark et al. (2011). These authors separated 385 coarse chromite grains (for definition see Ramdohr 1973) from recent chondrites classified as L/LL4, LL6, L4, L5, L6 and H4, H5, H6 by hydrofluoric acid treatment and sieving. Following separation Alwmark and collaborators scanned the chromite grains for inclusions using synchrotron radiation X-ray tomographic microscopy at the Swiss Light Source. Here, the two grains with inclusion Px incl. 1 and 2 were selected for cosmic ray track studies based on their large inclusions (~40 µm in diameter).

To proceed with the cosmic ray track study the grains had to be mounted in epoxy, and to confirm that the epoxy could withstand the harsh alkali treatment a test etching of a blank epoxy mount with apatite grains was carried out. The TIB granite described under 3.1 was first crushed and then density separated using a Wilfley shaking table (for detailed description on this mineral separation technique see Söderlund and

Table 3. The samples used for CRT studies in SEC grains.

Locality	Sample	Inclusion mineralogy	Etching conditions	Size inclusion	Reference
Hällekis	Golvsten E	Olivine	30+20 min WN*	~8 µm	Schmitz and Häggström 2006
Hällekis	Sextummen 1	Olivine	30+20 min WN	~5 µm	Schmitz and Häggström 2006
Lynna River	Ly1	Olivine	30 min WN	~8 µm	Lindskog 2011
Hällekis	Ark025 P2	Plagioclase	8min NaOH-solution¤	~3 µm	Lindskog 2011

*Krishnaswami et al. 1971
¤Lal et al. 1968

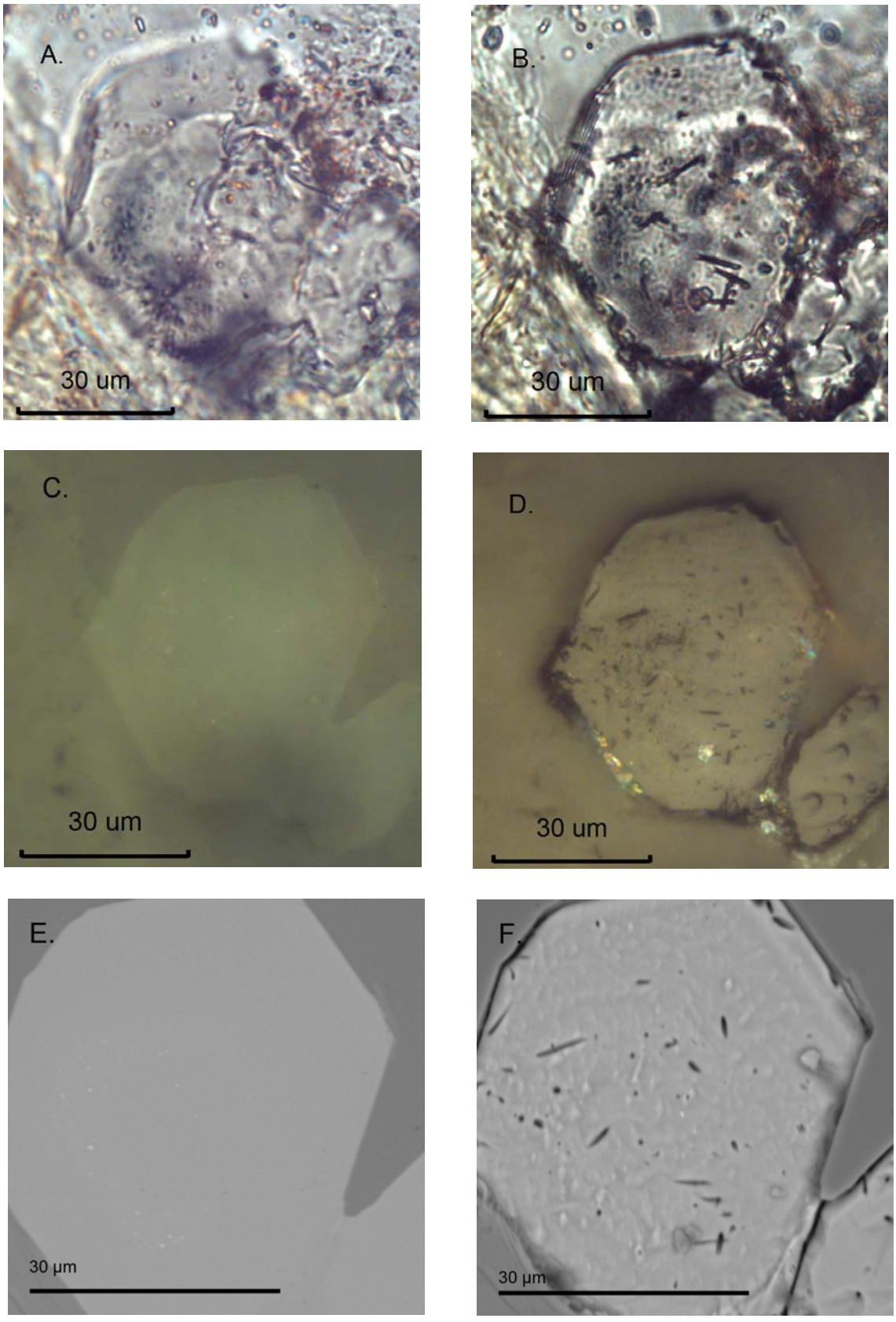

Fig. 9. Fission tracks in apatite in Siljan granite. Images to the left (A, C, E) are presenting the grain prior to etching, images to the right (B, D, F) were captured after etching for 20 s in 5M HNO_3 at room temperature. Image A-B shows the grain in transmitted light, images B-C with incident light, D-E are BSE micrographs. Fission tracks in terrestrial apatite are produced by spontaneous fisson of ^{238}U.

Johansson 2002). Apatite grains were picked from the high density fraction of the sample and mounted in epoxy. The grain mount was etched in a boiling solution of 6 g NaOH and 4 ml water for 30 min. It was found that the epoxy remained intact with all grains kept in place.

The two chromite grains with Px incl. 1 and 2 were mounted in epoxy resin and polished flat using 6 µm and 1 µm diamond slurry. The inclusions were relocated using SEM and carefully documented with BSE images. The grains were then etched in a boiling solution of 6 g NaOH and 4 ml water for 5 min using the reflux system (Lal et al. 1968; Fig. 8). After examination in the SEM the grains were etched for an additional 5 min. Only the surface of the grains is visible with BSE imaging and to verify that the etch pits are indeed nuclear tracks a documentation over how the etch pits behaved with increased depth was obtained by repeatedly polishing and documenting in the SEM. For the first sets of polishing only 1 µm diamond slurry was used. However, it was soon found that a short polish with 3 µm diamond slurry followed by 1 µm diamond slurry was preferable. After each polishing a set of BSE images were captured. When some of the tracks had disappeared the grains were etched for another 5 min and then successive polishing and photographing continued. The grains were etched for a total of 20 min.

In the BSE images the tracks are clearly visible as etch pits. In Adobe Photoshop CS5.1 the images from different levels in polishing were fitted onto each other based on the outlines of the inclusion and the fractures in the inclusion. The etch pits in each image were marked with dots and an image illustrating how the etch pits moved over the surface of the inclusion with increased polishing could be produced. To further establish that the etch pits moved as illustrated by the dots in the image two angles between the etch pits were measured in the images using Quartz PCI.

3.4 Cosmic ray tracks in silicate mineral inclusions in sediment-dispersed chromite grains

The samples used here had been prepared by Schmitz and Häggström (2006) and Lindskog (2011), Table 3. These authors had separated the chromite grains from limestone by leaching in acid, sieving and occasionally by heavy liquid separation. Chromite grains were picked out under the light microscope and then analyzed using an energy dispersive spectrometer fitted to the SEM (EDS; INCA x-sight, Oxford Instruments). Based on the chemistry of the grains they could identify the extraterrestrial chromite grains which were mounted in epoxy and polished flat. For this study the mounts with extraterrestrial chromite grains were systematically searched for inclusions using SEM. EDS was used to determine mineralogy of the inclusions. Four grains with suitable inclusions were found (Table 3). The carbon coating on the grains with suitable inclusions was polished away and the inclusions were carefully documented using BSE imaging in VPSEM. The grains were then etched; etching conditions are listed in Table 3, washed using tap water, distilled water and methanol (see 3.1 for detailed description) and documented again in the VPSEM.

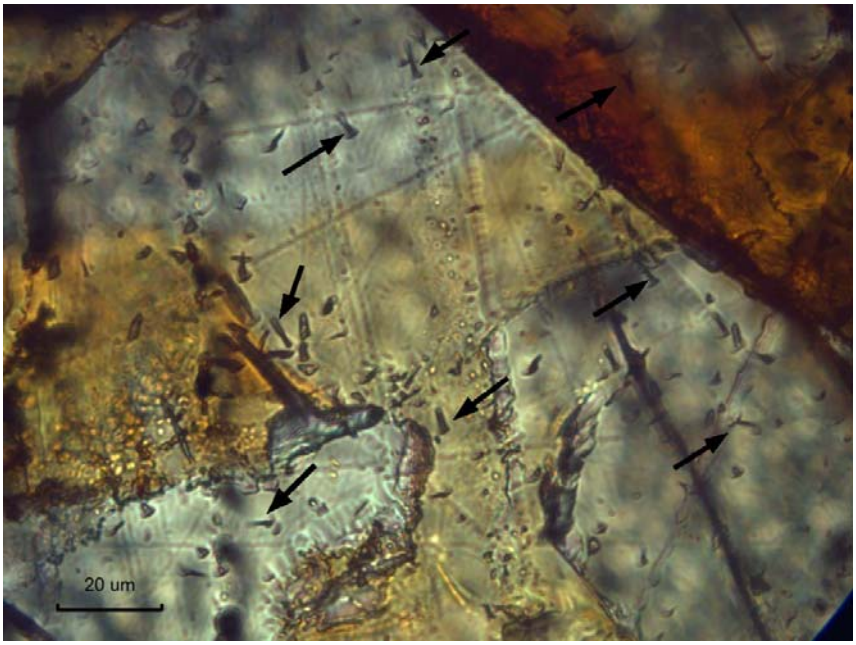

Fig.10. Cosmic ray tracks in Ozona 1 after 4h etching in a boiling solution of WN etchant. Some of the most well developed tracks are marked with arrows.

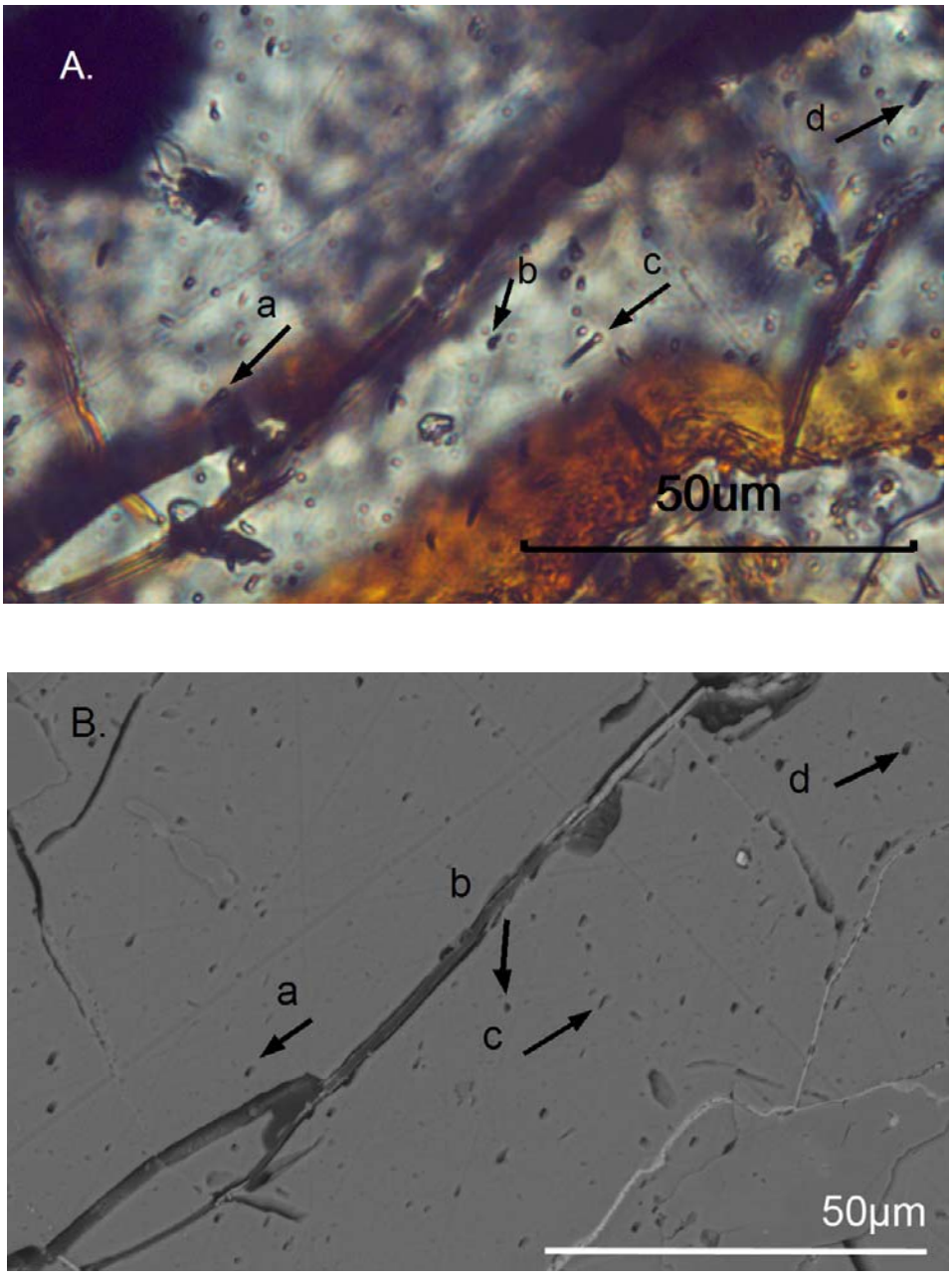

Fig. 11. Cosmic ray tracks in Ozona 3. Fig. 11a is an image in transmitted light of an olivine grain after two hours etching in WN solution, four well developed tracks are marked with a-d. Fig. 11b shows the same area after etching but with BSE imaging, tracks a-d are indicated in this image as well. Note how the etch pits are sub-circular for tracks with an high angle to the surface (e.g., track b) and more elongated for tracks which are more parallel to the grain surface (e.g., track c). Fig. 11c-d (page 17) show parts of another olivine grain in Ozona 3 with BSE imaging before and after etching. No defects are visible on the surface prior to etching (Fig. 11c). After etching numerous small etch pits appear (Fig. 11d). The etch pits in Fig. 11d are similar in appearance to the etch pits correlated to tracks in Fig. 11b.

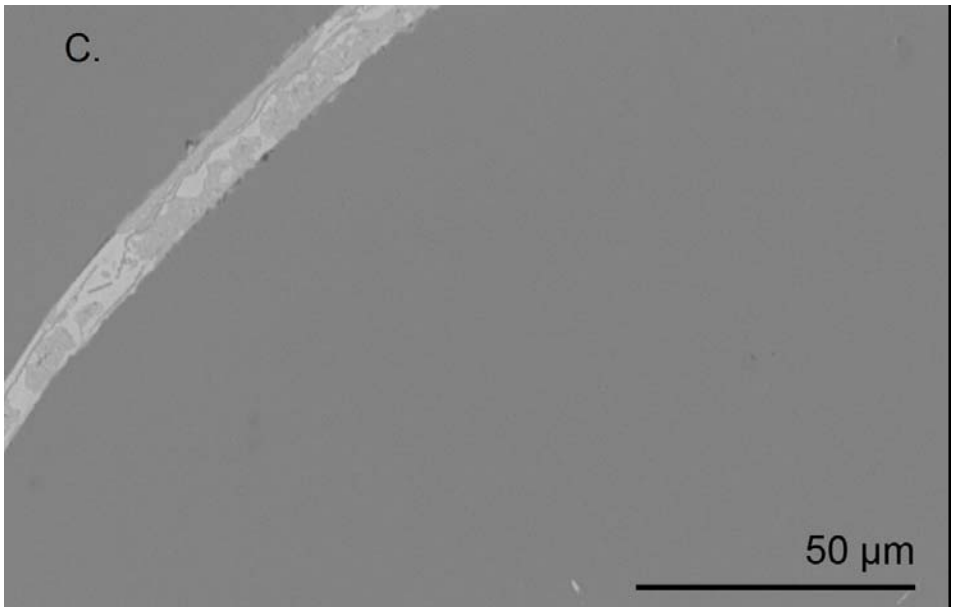

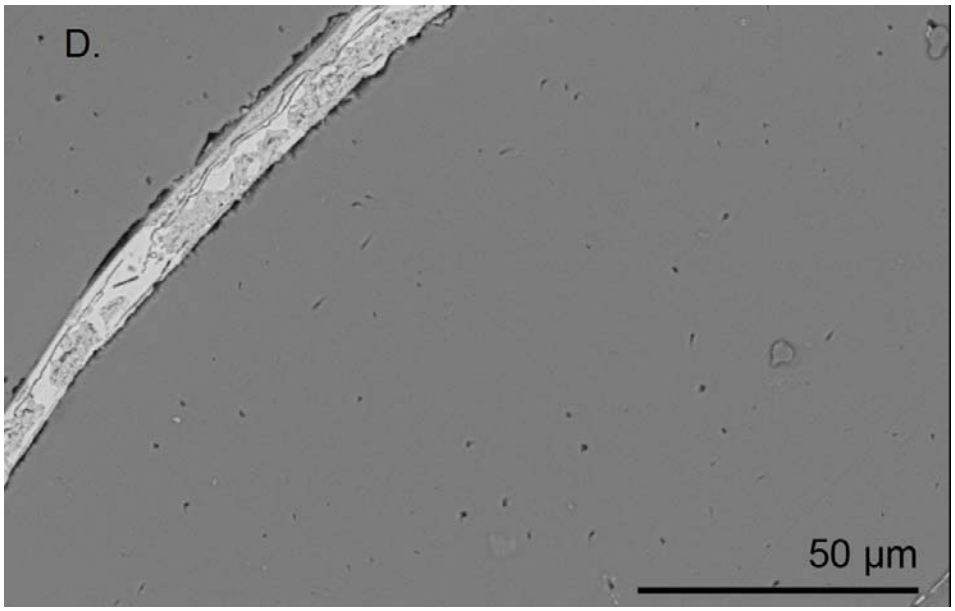

4 Results

4.1 Fission tracks in terrestrial apatite

Following etching, clear fission tracks appeared in the apatite grains (Fig. 9). In transmitted light the characteristic cone shape of the fission tracks is visible. The fission tracks appear as distinct features upon etching and are not related to any visible defects in the grain. In reflected light the tracks also became visible after etching although less pronounced than in transmitted light. In the BSE image the tracks appear as thin lines or more dot-like etch pits (Fig. 9).

4.2 Cosmic ray tracks in olivine, pyroxene, and merrillite from recent meteorites

Ozona 1 and Ozona 2 were etched for 4h in WN etchant, after which cosmic ray tracks became visible in olivine (Fig. 10). Tracks also appear after only two hours of etching (Ozona 3; Fig. 11), even though they are less well developed than after a full four hours etch. In BSE imaging no defects are visible prior to etching (Fig. 11 c), after etching numerous small etch pits appear (Fig. 11 d) which are similar in appearance to the etch pits correlated to tracks (Fig. 11 a-b). The track related etch pits differ in shape from more or less

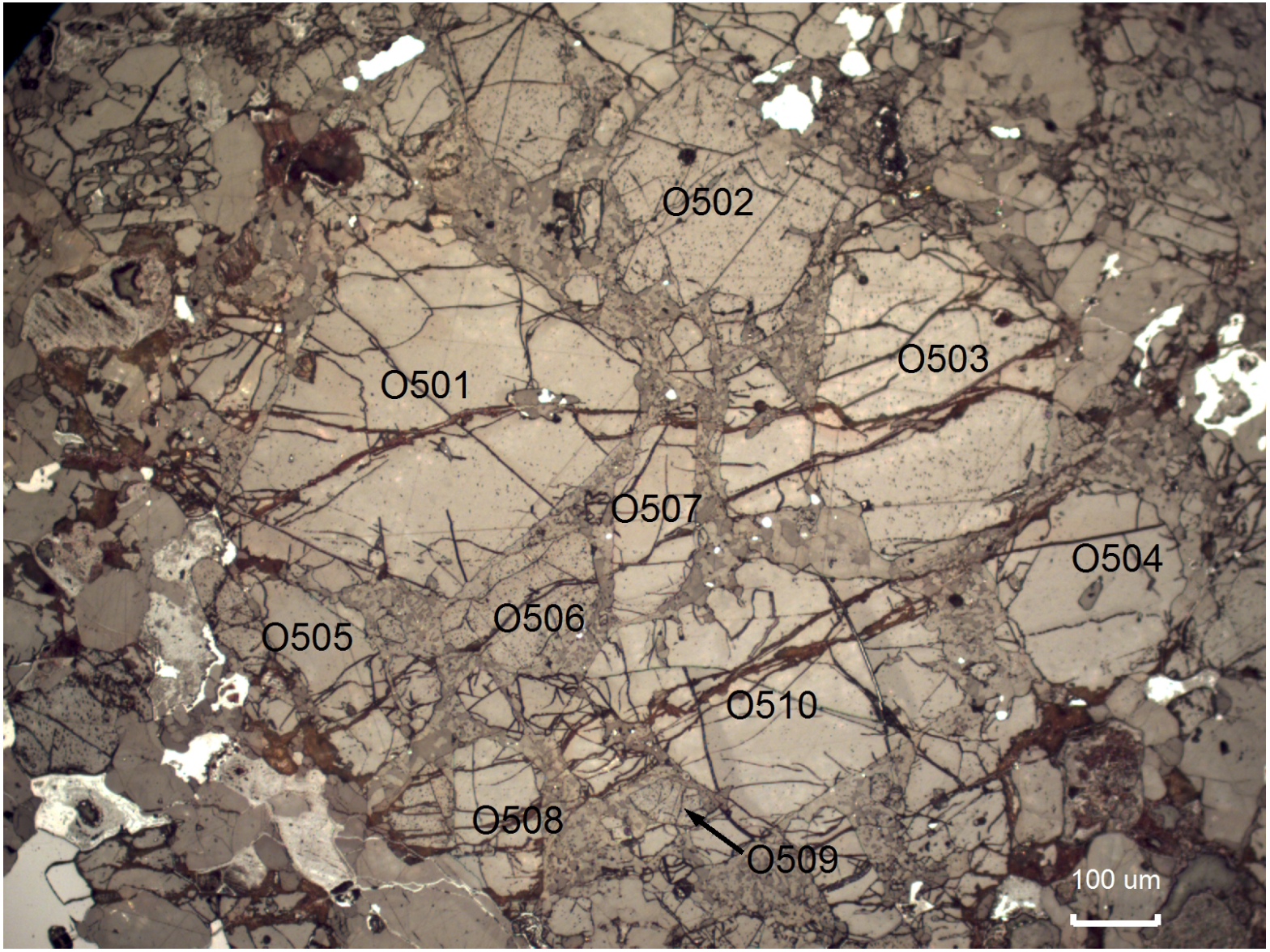

Fig. 12. Overview of a chondrule in Ozona 3 after etching in reflected light. Note how the different grains appear to have significantly different track densities. Etch pit densities were counted for grains O501 to O510.

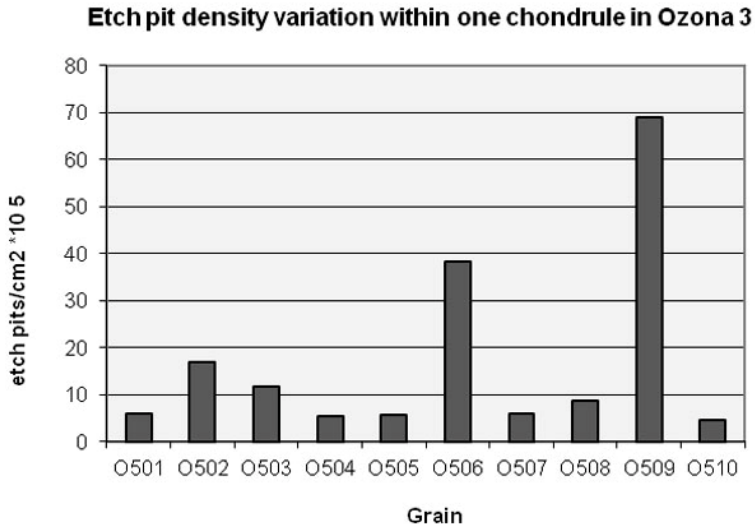

Fig.13. Showing the large etch pit density difference between different olivine grains in Ozona 3 (cf. Fig. 12). The etch pit densities were counted in BSE images using 900x magnification. The areas of the grains were calculated using Quartz PCI.

Table 4. Etch pit density measurements in olivine grains from one chondrule in Ozona 3.

Grain	Area measured (cm^2)	#etch pits	Etch pits/cm2 $*10^5$
O501	0.000876	514	5.9
O502	0.000371	626	16.9
O503	0.000477	563	11.8
O504	0.000260	139	5.3
O505	0.000163	91	5.6
O506	0.000161	618	38.4
O507	0.000171	100	5.8
O508	0.000078	69	8.8
O509	0.000031	214	69.0
O510	0.000456	209	4.6

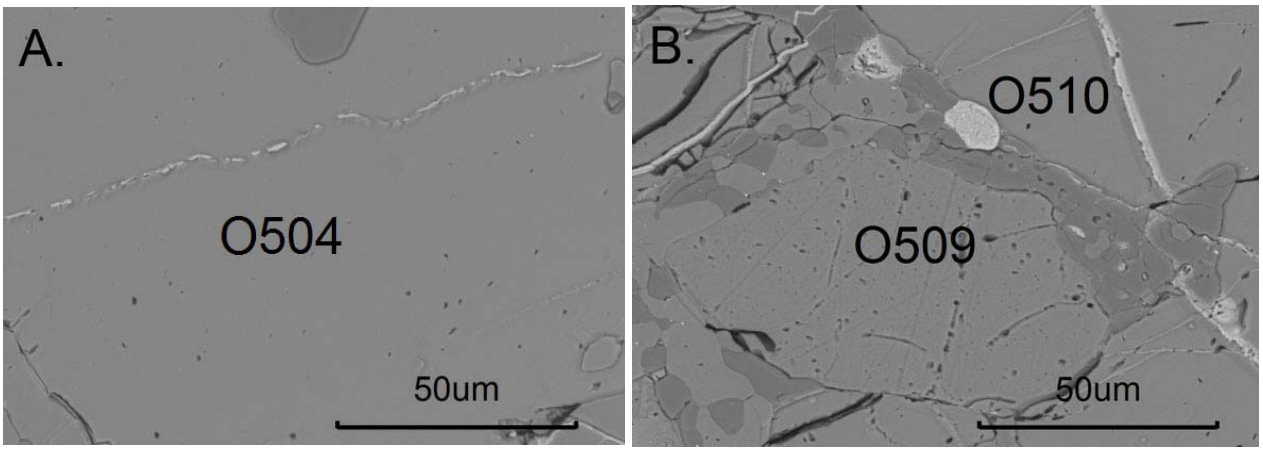

Fig. 14. BSE images showing difference in etch pit density between olivine grains within the same chondrule. (Parts of) three grains are visible in these images; the two low etch pit density grains O504 and O510, and the high etch pit density grain O509. Grain O509 have a higher density of fractures than the two other grains, perhaps are also some of the etch pits in O509 less well constrained than the etch pits in O504 and O510.

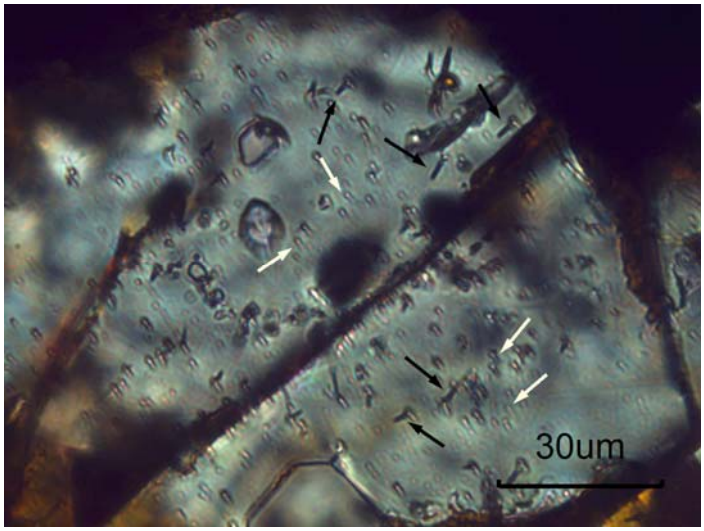

Fig. 15. Part of an olivine grain in Ozona 3 after etching. Two types of etch pits are present, interpreted as GCT (some examples are indicated with black arrows) and other defects in the crystal not related to cosmic rays (some examples are indicated with white arrows).

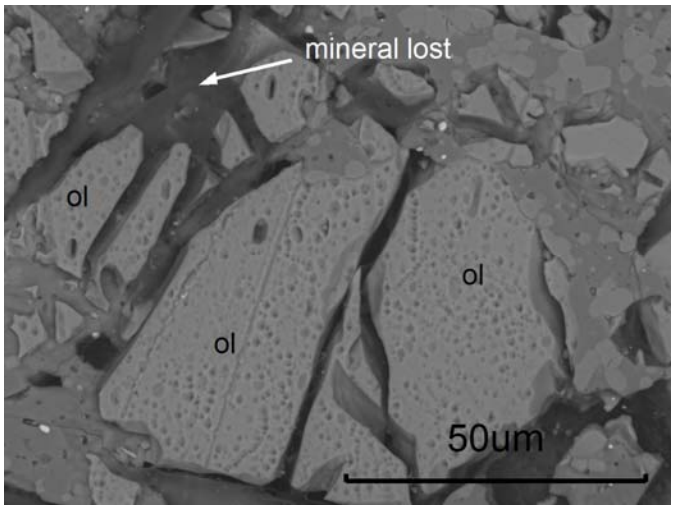

Fig. 16. BSE image of Holbrook 1 after 4h etching in WN etchant. Parts of olivine grains are marked with "ol". Some parts of the thin section were lost. The surfaces of the olivine grains are completely covered with etch pits.

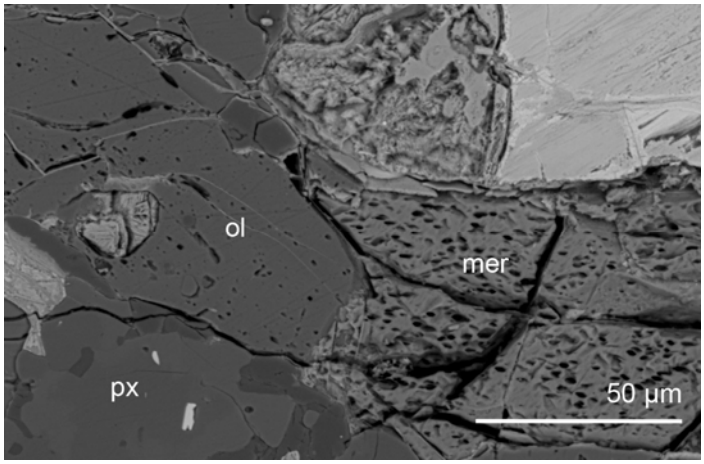

Fig. 17. BSE image of Ozona 3 after two hours of etching in boiling WN solution. Three minerals with the potential to register CRT are present in the image; merrillite (mer), olivine (ol) and pyroxene (px). The merrillite has a considerably higher track density than the olivine due to the presence of fission tracks from fission of mainly ^{244}Pu in this mineral. The pyroxene is unaffected by the WN esolution which was developed mainly as an olivine etchant.

circular to elongated. Another interesting feature in Ozona 3 was that olivine grains within the same chondrule had different etch pit densities (Fig. 12, 13, 14; Table 4). The difference in etch pit densities is visible in an overview of the chondrule (Fig. 12) and confirmed by calculating etch pit densities in BSE images (900x magnification) of individual olivine grains in the chondrule (Fig. 13 and Table 4). The grains with high etch pit density also have higher densities of fractures than the grains with lower etch pit density (cf. grain O509 with grain O504 and O510 in Fig. 14). All points towards that the difference in etch pit density in fact does not correspond to a difference in GCT density, instead the additional etch pits in some of the grains are produced by defects in the crystals. An interpretation that is further confirmed by Fig. 15 in which it is clear that there are two types of defects in the olivine; GCT and other defects which all have same direction.

The Holbrook (L/LL 6) sample was etched for 4h in WN etchant. Large parts of the olivine grains in the sample were destroyed during etching. The surfaces of the grains which remained relatively intact are covered with etch pits (Fig. 16).

The WN etchant reveals tracks in phosphate minerals in addition to olivine (Fig. 17; Pellas and Storzer 1981). The track density in the merrillite in Ozona 3 is considerably higher than track density in olivine due to the contribution of fission tracks mainly formed by the now extinct isotope ^{244}Pu. Pyroxene is apparently unaffected by the WN etchant (Fig. 17). To reveal tracks in pyroxene Ozona 4 was etched for 5 min in a boiling solution of NaOH and water as described by Lal et al. (1968) for track etching in pyroxene. The short etch only represents 1/8 of full etching time in pyroxene, however, this was enough for large parts of the thin section to fall off the glass. The epoxy in the thin section was not resistant enough for etching in boiling NaOH solution. Lal et al. (1968) recommend

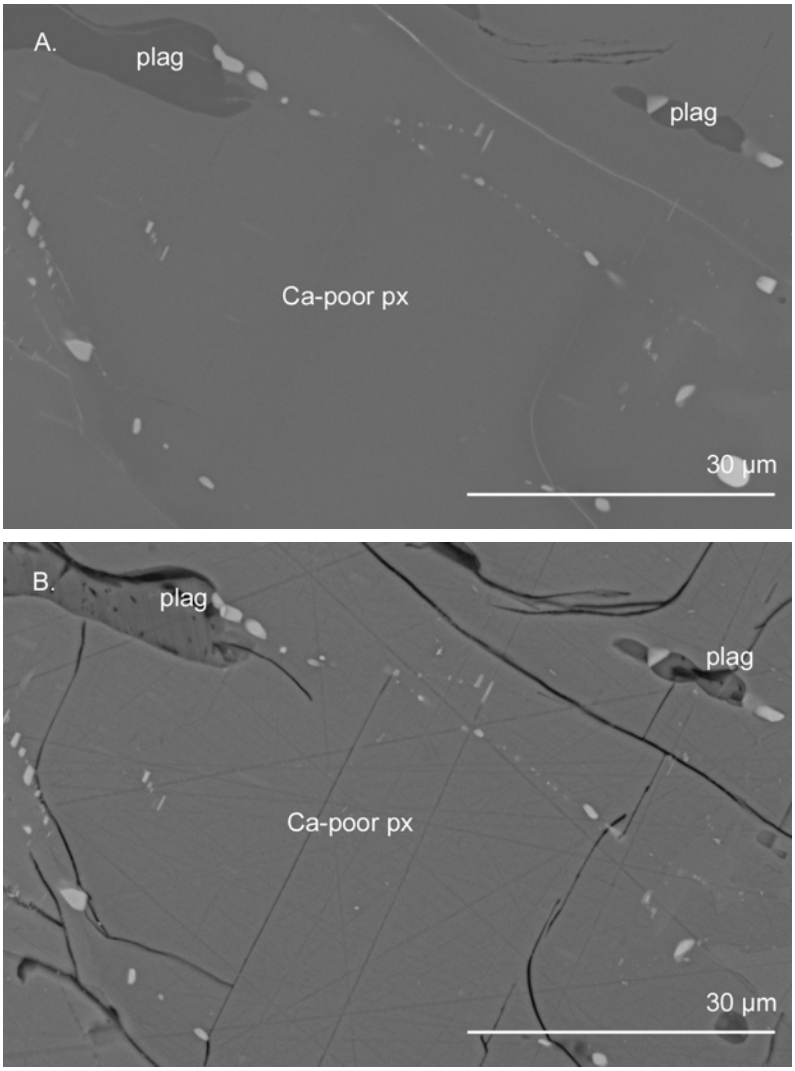

Fig. 18. BSE images of Ca-poor pyroxene (Ca-poor px) and plagioclase (plag) in Ozona 4 prior (A.) and after (B.) 5 min etching in a boiling NaOH-solution. Some polishing cracks became enlarged in the pyroxene, however, the etch was too short for any GCT to appear in the pyroxene. Well defined etch pits were developed in the interstitial plagioclase, which is more sensitive to the etchant than pyroxene.

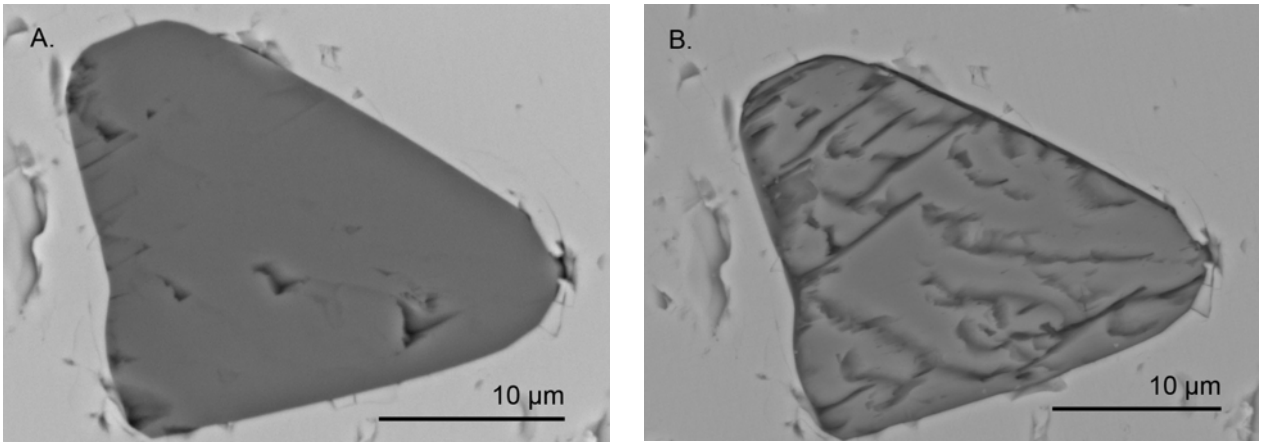

Fig. 19. BSE images of a Ca-poor pyroxene inclusions (Px incl. 2) in chromite from Kernouvé prior (A) and after (B) 10 min etching in a boiling NaOH-solution. Extensive defects, which are likely to hide any cosmic ray tracks that are present in the inclusion, appeared on the surface of the inclusion after etching.

the usage of an alkali proof epoxy for this treatment. For track studies in the future it is recommended to always prepare samples with alkali proof epoxy. No tracks became visible in the pyroxene after only five minutes etching, however, tracks did appear in interstitial grains of plagioclase (Fig. 18). Plagioclase is typically etched in a more diluted boiling solution of NaOH and at shorter times than pyroxene (Lal et al. 1968).

4.3 Cosmic ray tracks in silicate mineral inclusions in recent chondritic chromite

After the first 10 min of etching several defects became enlarged in Px incl. 1 and 2 in chromite grains from Kernouvé (H6). In Px incl. 2, defects such as cracks and chips obscured a significant part of the inclusion after etching and no tracks were visible (Fig. 19). In Px incl. 1 seven nuclear tracks (FT or GCT, se discussion below) became visible after 10 min etching (Fig. 20). Following several sets of polishing an additional etch pit appeared which had previously been concealed by a chip on the surface of the inclusion. Hence, a total of 8 nuclear tracks are present in Px incl. 1.

The etch pits that are interpreted as tracks differ from other defects in that they have more well defined outlines and are often smaller than other defects, typically less than 1 µm large. The appearance of the etch pits differ slightly between tracks (Fig. 21); some etch pits are more elongated (Fig. 21 a) and others are almost circular (Fig. 21c). Etch pits also differ in size and the etch pit below the crack in Fig. 21 c is considerably larger than the one above the crack. The hole above the crack disappeared completely in the last polishing before the sample was re-etched, whereas the etch pit below the crack was still visible. Etch pits that did not fully disappear in between etchings are larger than etch pits that were polished down to such a degree that they were no longer visible in the SEM.

In addition to the tracks, other defects in the inclusions became enlarged through the etching. In Px incl. 2 such defects were so prominent that no tracks were visible (Fig. 19). In Px incl. 1 defects that masked the tracks appeared following re-etching after several sets of polishing (cf. Fig. 20 c and d). In contrast to the nuclear tracks the "new" defects were shallow and disappear after some polishing.

The movement of the intersection between the etched tracks and the surface of the inclusion with increased polishing of the grain, i.e. when moving downwards in the grain, is illustrated in Fig. 22. The image in the background shows the grain after the first etching and before any extensive polishing. The white dots are located on the tracks in this image. Successively darker dots then mark the locations of the tracks on the grain surface as the grain was polished down. For example; the two tracks at the upper left side of the inclusion move towards the edge of the inclusion as the sample is polished down. The intersections of tracks with the surface of the inclusion all move in straight lines. The tracks have slightly different directions, even though the intersections of the tracks with the surface of the grain all seem to shift towards the upper part of the image and/or the left side of the image while moving downwards in the grain. The etch pits that move a lot between polishing sets also have a more elongated appearance (cf. Fig 21).

To further test that the intersection of the tracks and the surface indeed move as outlined in Fig. 22 two angles between etch pits in the images were measured (Fig. 23). Angle α increases as one moves downwards in the inclusion and angle β decreases as one moves downwards in the inclusion (Table 5). The etch pit furthest to the right in the angle β measurements appeared after some polishing. Hence, the variation of angle β is confirmed with fewer measurements than angle α. The measurements of the angles are in good agreement with the expected values for tracks that are located as illustrated in Fig. 22.

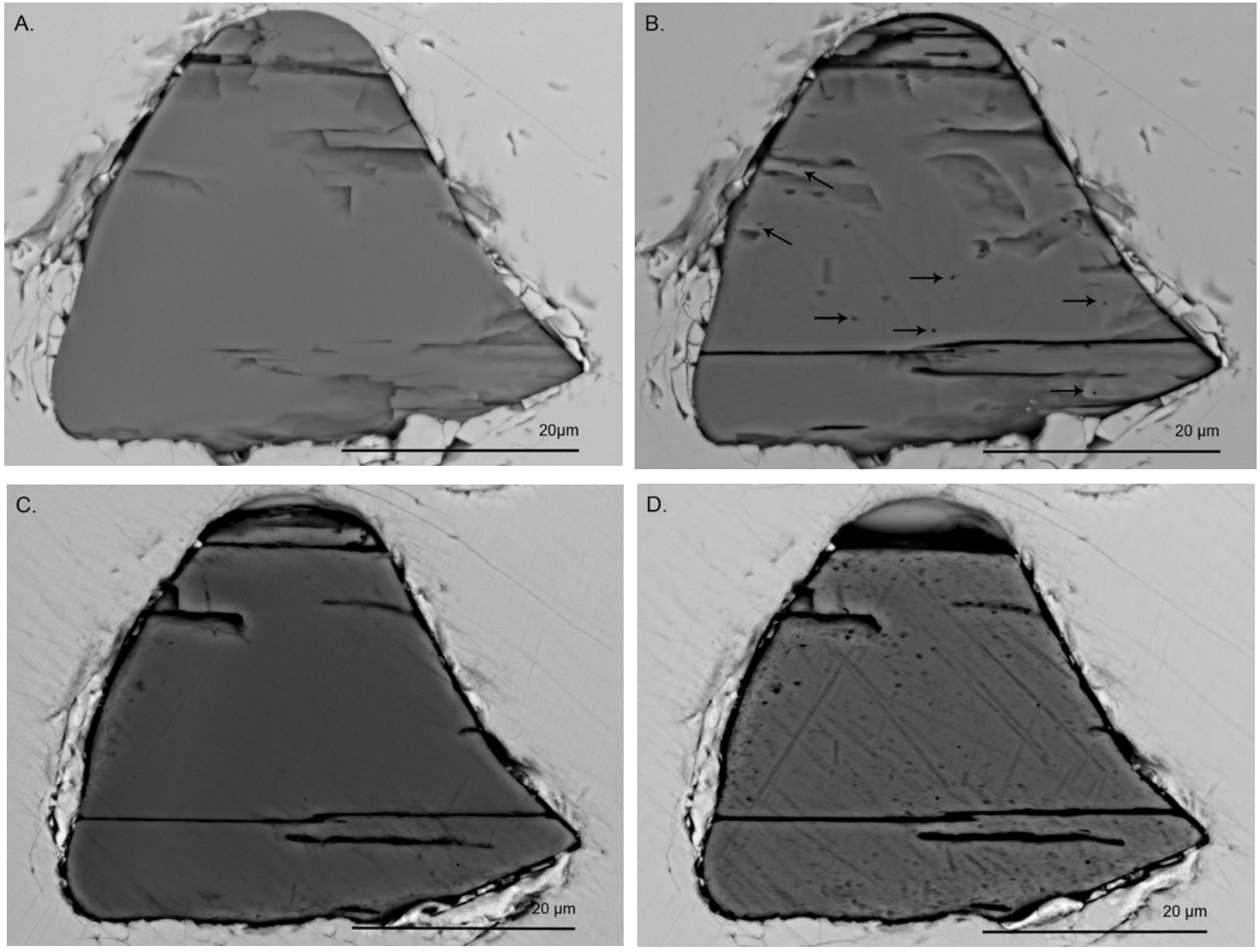

Fig. 20. BSE images of a Ca-poor pyroxene inclusions (Px. Incl. 1) in chromite from Kernouvé (H6). Image a shows the inclusion before etching, image b after the first 10 min of etching and before any additional polishing, image c after 10 min etching and extensive polishing, and image d shows the sample after 5 min re-etching. This set of images mainly illustrates two things; firstly, how etch pits related to nuclear tracks (indicated with arrows in b) and other defects appear after etching (b), disappear after polishing (c) and then reappear after re-etching (d). Secondly, the images illustrate the problem with defects induced by polishing. In image b, a few cracks are present which might conceal tracks, but the surface between the cracks is smooth. Tracks can easily be detected on these surfaces since there are few other defects. In image c, many of the superficial cracks and also about half of the track etch pits had been polished away. After re-etching, the nuclear tracks reappeared and several other defect also appeared which make it hard to detect the track etch pits in image d. These defects were shallow and disappeared after some polishing; they were most likely induced by the extensive polishing of the sample.

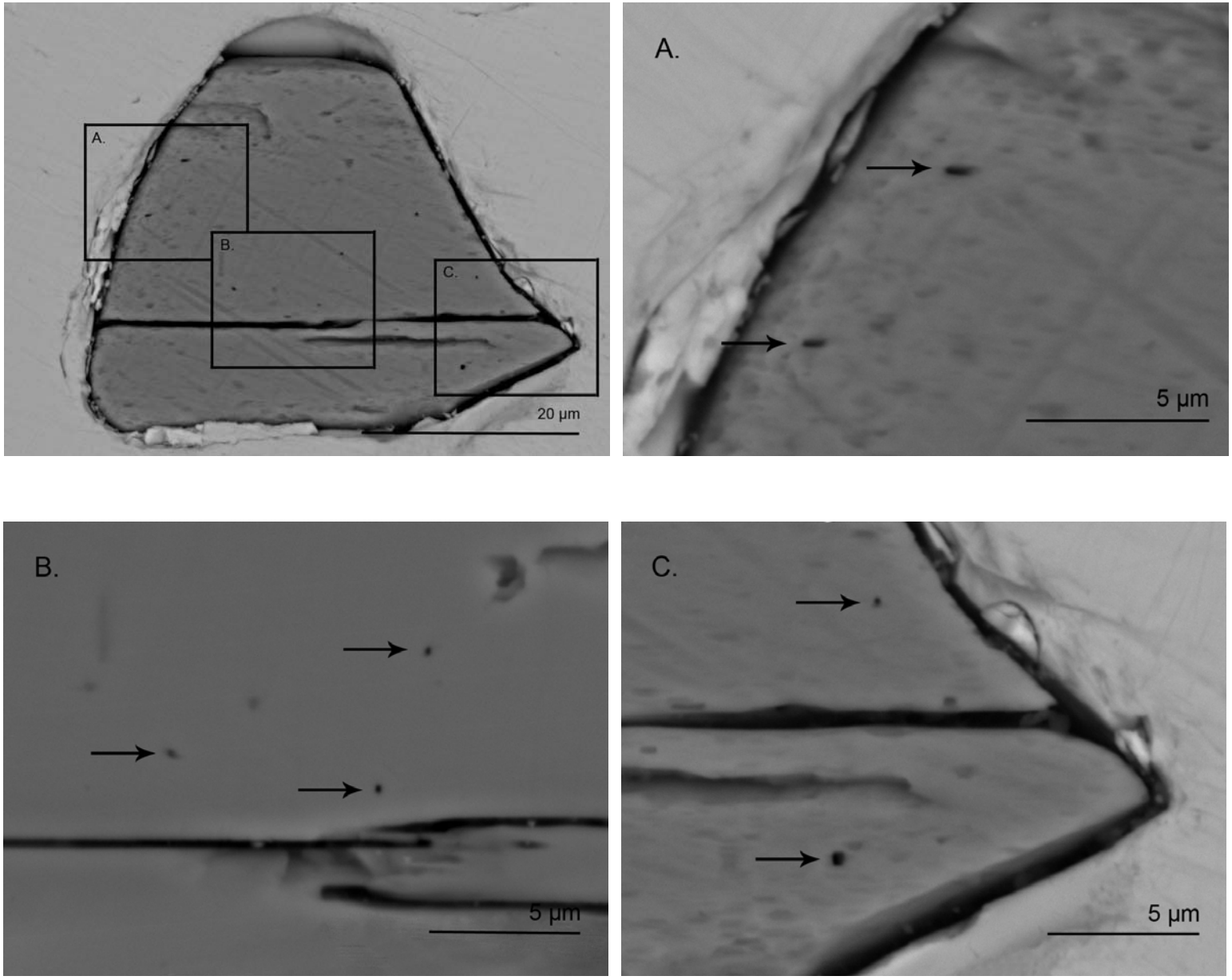

Fig. 21. BSE images of a Ca-poor pyroxene inclusions (Px. Incl. 1) in chromite from Kernouvé (H6). Close up images of three areas in the inclusion. The overview and image a and c were captured after 15 sets of polishing and a total of 20 min etching. Image b was captured after 10 polishing sets and 10 min etching. The tracks are visible as black dots on the images and indicated with arrows. The tracks in image a and the track furthest to the left in image b are more elongated than the other tracks. The tracks which are more elongated are also the ones that move most with increased polishing (cf. Fig. 22) and are interpreted as being more parallel to the surface of the inclusion than the tracks which have a more dot-like appearance and move less when polished. In image c two tracks are visible, one above the crack and one below the crack. The track etch pit below the crack is considerably larger than the track etch pit above the crack. The track above the crack disappeared completely in the last polishing before the sample was re-etched, whereas the track below the crack was still visible.

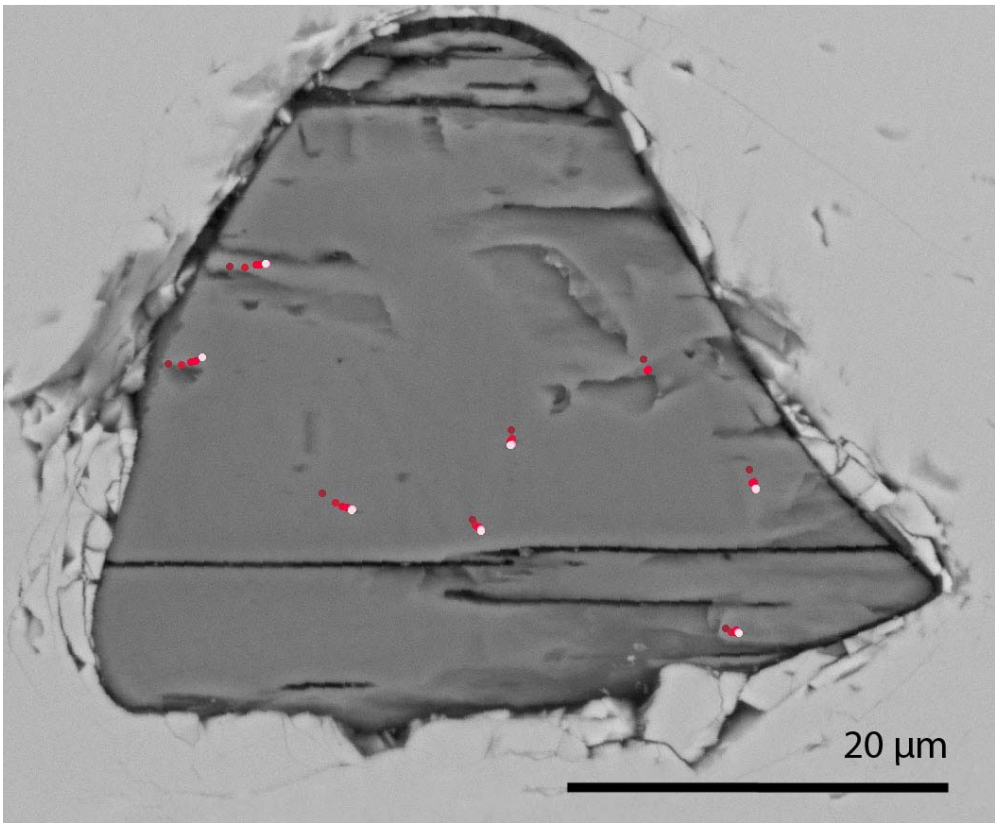

Fig. 22. BSE image of a Ca-poor pyroxene inclusion (Px. Incl. 1) in chromite from Kernouvé (H6), superimposed on the image are the locations of the track etch pits after 6 sets of increasing polishing. The image in the background shows the grain after the first etching and before any extensive polishing. The white dots are located on the tracks in this image, successively darker dots then mark the locations of the tracks on the grain surface as the grain was polished down. For example; the two tracks at the upper left side of the inclusion move towards the edge of the inclusion as the sample is polished down. The intersections of tracks with the surface of the inclusion all move in straight lines. The tracks have slightly different directions, however, all track etch pits have a preferred orientation towards the upper part of the image and/or the left side of the image with increased depth.

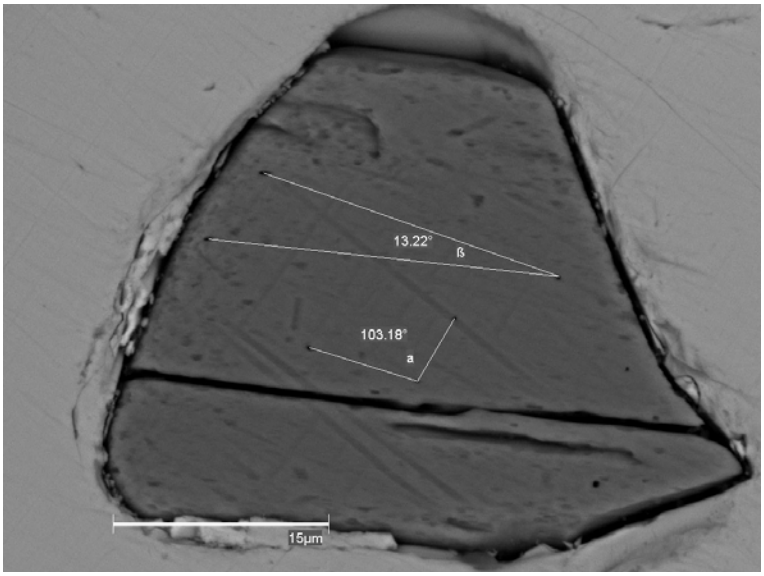

Fig. 23. BSE image of a Ca-poor pyroxene inclusions (Px. Incl. 1) in chromite from Kernouvé (H6). Angle α and angle β were measured, using Quartz PCI, in images captured after successively increasing polishing to confirm that the etch pits moved as illustrated in Fig. 22 in-between polishing sets. The image shows the measurement of "polish 7" (c.f. Table 5).

Table 5. The angles in Fig. 23 measured in images captured after successively increased polishing.

	polish	Angle (°)
α	1	99.7
	2	100.2
	3	100.3
	4	100.7
	5	101.7
	6	102.7
	7	103.2
β	4	14.0
	5	13.9
	6	13.7
	7	13.2

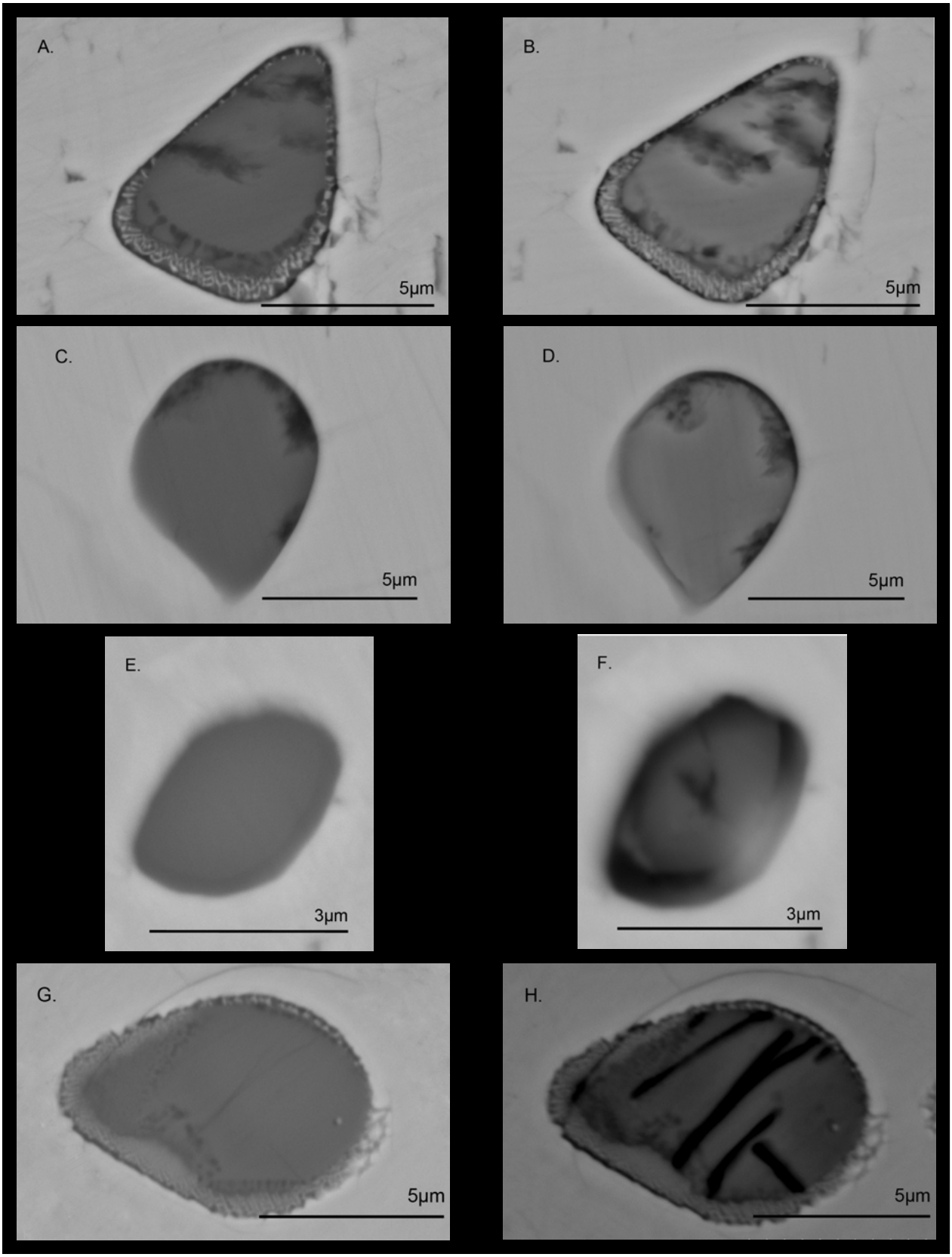

Fig. 24. BSE images of inclusions in four SEC grains before (to the left) and after (to the right) etching. Fig. 24 a-b is an olivine inclusion from Golvsten E, CFig. 24 c-d shows an olivine inclusion from Sextummen 1, Fig. 24 e-f is the plagioclase inclusion in Ark025, and Fig. 24 g-h is the olivine inclusions in Ly 1. Cosmic ray tracks did not appear in any of the inclusions upon etching. All samples show signs of being affected by the etching, but to different degrees.

4.4 Cosmic ray tracks in silicate mineral inclusions in sediment-dispersed chromite grains

Tracks were not detected in any of the four SEC grains which were etched for cosmic ray tracks (Fig. 24). All samples were affected by the etching, but to different degrees. In Golvsten E (Fig. 24 a-b) and Sextummen 1 (Fig. 24 c-d) the cloud like impurities became slightly enlarged. However, the differences before and after etching are more obvious in Ark025 (Fig. 24 e-f) and Ly1 (Fig. 24 g-h). In the Ly1 inclusion the fractures that are hardly visible prior to etching are enlarged and clearly visible after etching. In Ark025 darker areas are visible at the edges of the inclusion after etching and there are also two lines intersecting each other at the centre of the inclusion.

5 Discussion

5.1 Nuclear tracks in minerals and in silicate mineral inclusions in chromite

Even though a full etching time is required for proper development of tracks in their full etchable track length (Fleischer et al. 1975), tracks are visualized after considerably less etching time as illustrated in Ozona 3 (50 % full etching time; Fig. 11) and also in Px incl. 1 in chromite from Kernouvé (~ 25 % full etching time; Fig. 21). For track studies in inclusions in chromite a short etch is preferable over a long etch since defects will be less developed.

Track studies are extremely sensitive to the quality of the crystals in which such studies are carried out, and the work in this thesis clearly illustrates the importance of the quality of crystals for successful track studies. The tracks constitute defects in the crystals and are difficult to detect if there are other defects present concealing them. The reason for the poor results with thin section Holbrook 1 was that large parts of the thin section were destroyed during etching (Fig. 16), this could either be due to poor quality of the olivine crystals in Holbrook 1 as compared with olivine in Ozona (1-3), or due to a considerably higher track density. The etch-pit covered surface in Fig. 16 indicates that Holbrook 1 had very high track density, such surfaces could on the other hand also be produced by defects in the crystals, as illustrated by Ozona 3 (Fig. 12 and 14) where apparent track densities varies considerably (Fig. 13). It is not likely that the apparent higher track densities in some crystals in Ozona 3 is a consequence of pre-irradiation in the parent body regolith since the high track density crystals occur in the same chondrules as the crystals with lower track densities (cf. Metzler 2004).

GCT are present in Px incl. 1 in chromite from Kernouvé. This is the first time that CRT are detected in silicate mineral inclusions in chondritic chromite and a clear indication that it should be possible to find CRT in silicate mineral inclusions in SEC grains. It might be argued that the tracks in Px incl. 1 are fission tracks and not GCT. Such an objection would be based on the presence of U or other fissionable elements in pyroxene. These concentrations are usually quite low, in the range of 10^{-2} ppb by weight (Lal 1969 and references therein). Still, it is a concentration high enough to make contribution of fission track densities become important at a depth of around 15-20 cm (Lal 1969) and the depth of the sample is unknown. One, or even a few, of the tracks in Px incl. 1 might be FT. However, it is highly unlikely that all the tracks in the inclusion are FT based on (1), the usually low concentration of U in pyroxene, and (2) the anisotropy of the tracks in the inclusion. FT always have an isotropic distribution due to the random distribution of radioactive isotopes (Crozaz et al. 1970). No CRT were found in the four silicate mineral inclusions in SEC grains from mid-Ordovician, 470 Myr old, sediments which were etched for tracks in this study, even though the GCT in Px incl. 1 indicates that it should be possible to find CRT in SEC grains.

5.2 Why were no cosmic ray tracks found in inclusions in sediment-dispersed extraterrestrial chromite grains?

There are four possible explanations for the lack of CRT in the inclusions: firstly; the condition of the grains, secondly; that there were no tracks in the inclusions to start with, thirdly; that the composition of the inclusions did not match the etchant and, finally; annealing of the tracks during atmospheric entry and/or sediment burial.

The first explanation for not finding any tracks in the inclusions is that the inclusions were too damaged by other processes to detect tracks. The fact that no tracks appeared in Px incl. 2 from Kernouvé is best explained by the large amount of cracks in the inclusion which efficiently would obscure any cosmic ray tracks (Fig. 19). The two grains with Px incl. 1 and 2 come from the same small (10-20 g) piece of Kernouvé (C. Alwmark pers. comm. 2011-11-21). Hence, it is unlikely that the two grains would have significantly different cosmic ray track densities. The importance of the quality of the sample in any track study is also clear from track studies in silicate minerals from recent meteorites (see 4.2 and 5.1), and cannot be emphasized enough. With this background, poor quality of the inclusions could very well explain that no tracks were found in the SEC grains inclusions, for example, any tracks in the Ly1 sample (Fig. 24 g-h) would be efficiently obscured by the large cracks. On the other hand, Sextummen 1 (Fig. 24 c-d) only holds minor defects and the quality of the crystals alone cannot explain that no tracks were found in the inclusions of the SEC grains.

The second possible explanation for not finding any tracks in inclusions is simply that there were no tracks to start with. Of greatest importance for a successful outcoming in this project is that inclusions

are large enough to make it probable to detect tracks in them. Even though the largest inclusions that were found were used, the inclusions were small if compared with Px incl. 1 and 2 from Kernouvé. The inclusions in SEC grains had a largest dimension between 3 and 8 µm, whereas Px incl. 1 and 2 measured ~40 µm. The small sizes of the inclusions make it less probable to find tracks in them. There is also the possibility that the micrometeorites had been subjected to cosmic rays for such a short time that it is unlikely that tracks would develop.

Another possible explanation that no tracks were found in the SEC grains inclusions is that the etchant didn't work on the inclusions. The inclusions in Ly 1 (olivine) and Ark025 (plagioclase) were clearly affected by the etchant and it can be concluded that the etchant matched the chemistry of the mineral. However, in Golvsten E and Sextummen 1 (both olivine) the inclusions were less obviously affected by the etchant, even though they were etched for longer time than Ly1 (50 min compared to 30 min for Ly1). One possible explanation for the lack of tracks in these two inclusions could be that the compositions of the inclusions fall outside of the range under which the etchant works efficiently. The WN etchant was used for Golvsten E and Sextummen 1. It develops tracks properly in olivine with a fayalite component of 15-30 % (Krishnaswami et al. 1971). The inclusions were too small to carry out satisfying analysis with simple EDS analysis. Alwmark and Schmitz (2009) did more profound work on the elemental composition of olivine inclusions in chondritic chromite and found that slight differences were present between compositions of the inclusions and olivine in the matrix. They found that the inclusions had elevated chromium content and on an average 14% lower faylite content that the olivine in the matrix. The lower fayalite content found in inclusions compared to the composition of olivine in the matrix might affect olivine inclusions in H chondrites so that the WN etchant is not ideal. Even though this is one plausible explanation for not finding any tracks in Golvsten E and Sextummen 1 it is not the most likely, mainly since the SEC grains in Hällekis are expected to predominantly be of L-chondritic origin (Schmitz et al. 2001; Schmitz and Häggström 2003; Bridges et al. 2007). The same batch of WN solution was used for Golvsten E and Sextummen 1 and the possibility that something was wrong with the batch cannot be excluded. In fact the etchant behaved differently as compared with previous etchings in WN solution while it was boiling, indicating that something might have gone wrong during the preparation of the solution.

The fourth explanation for the lack of tracks in inclusions in SEC grains is that tracks were annealed during atmospheric entry or sediment burial. For annealing of tracks in micrometeorites not to occur during atmospheric entry special conditions need to be fulfilled (Love and Brownlee 1991). Bradley et al. (1984) found SFT in IDPs collected from the stratosphere. However, Bradley and collaborators only found SFT in two out of five investigated IDPs. Hence, it is not unlikely that tracks in at least some of the SEC grains were annealed upon atmospheric entry. It is also possible that tracks in inclusions in chondritic chromite were annealed while the grains were buried as an affect of elevated temperature and pressure. Conodont Alteration Index (CAI) for the Hällekis section is 1 and the conodont specimens are very well preserved (Mellgren and Eriksson 2010). A CAI of 1 means a heating of at the most 80°C (Königshof 2003). Pressure is always less important as track annealing process than temperature in settings with normal geothermal gradient (Fleischer et al. 1975 and references therein). Based on the data presented in 2.6.2 it is not likely that cosmic ray tracks in olivine and plagioclase are annealed at temperatures lower than 100°C. Hence, it is not likely that the tracks in the three samples from Hällekis had been annealed during sediment burial.

5.3 Suggestions for further studies

Theoretically it should be possible to find cosmic ray tracks in silicate mineral inclusions in SEC grains from the Hällekis section. The fact that GCT were found in Px incl. 1 from Kernouvé (H6) and that SFT previously have been found in IDPs collected from the stratosphere (Bradley et al. 1984) further corroborate this. However, for such searches to be successful it is essential that large, well preserved, inclusions are used. Large inclusions in chromite grains could be detected using synchrotron radiation X-ray tomographic microscopy, as done for chromite grains from recent meteorites by Alwmark et al. (2011). Large inclusions could then be etched for tracks or investigated using TEM. Due to the small size of the inclusions TEM could be preferable over etching and SEM, partly since tracks could be seen as tracks rather than etch pits. Further, if the inclusions are properly calibrated using heavy ion accelerators and partial annealing processes fully understood it could also be possible to determine the track producing element if the tracks are measured, opening up for the possibility to reconstruct the cosmic ray beam over a geological time scale. The motion of Earth relative the galactic spiral arms occurs on a 100 Myr timescale (Shaviv 2002). Micrometeorites are expected to have a maximum transit time of 2.2 Myr from the asteroid belt to Earth (Meier et al. 2010 and references therein) and comparing cosmic ray track densities in silicate mineral inclusions in SEC grains from different levels in the geological record could give insight into fluctuations in the cosmic ray beam. One weakness of this approach is that grains in micrometeorites can have been pre-irradiated in the protoplanetary nebula or in a regolith breccia, in fact Meier et al. (2010) found that a large fraction of SEC grains from Kinnekulle had been pre-irradiated in regolith breccias. The problem with pre-irradiated grains could be circumvented by analyzing noble gas isotopic ratios in the grains which

would allow for distinguishing regolith breccia grains from other grains. Another problem which needs to be solved if this project is to be successful is how to distinguish SFT from GRT in inclusions in the SEC grains.

6 Conclusions

Cosmic ray tracks are recorded in silicate mineral inclusions within chondritic chromite. This is clear indications that it should be possible to find cosmic ray tracks in sediment-dispersed extraterrestrial chromite (SEC) grains. No tracks were found in the four inclusions in SEC grains that were etched for tracks here. Several factors have to work together for cosmic ray tracks to be preserved in SEC grains; firstly inclusions have to be large enough to make it probable for tracks to be recorded, secondly the inclusions have to be subjected to cosmic rays for enough time to make cosmic ray track recording probable, thirdly cosmic ray tracks are not to be annealed during atmospheric entry or later during their history at Earth and finally the inclusions have to be in such a good condition that no other defects are to obscure the cosmic ray tracks. Successful searches of cosmic ray tracks in SEC grains are therefore most likely based on larger sample sets than what was used here. Scanning the SEC grains with synchrotron radiation X-ray tomographic microscopy would ensure that all large inclusions in the batch are detected.

7 Acknowledgments

I would like to express my gratitude to my supervisor Birger Schmitz for initiating and showing great dedication to this project, and for providing me with everything from lab equipment and samples to comments on my drafts. Special thanks also to my co-supervisor Carl Alwmark, not only for providing me with insightful comments throughout this work, reading my drafts and providing me with material, but also for being a great support during the more trying episodes in the project. Thanks also to Knut Metzler and Rainer Wieler for enlightening discussions in the subject, to Sanna Holm for reading my draft and giving me access to her Siljan samples and to Anders Lindskog for letting me use the Lynna River samples. Last, but not least, I would like to thank Anders Cronholm for helping me with practical issues, Linnea S Arbab for guiding me through the secrets of Photoshop and everybody else who have been helpful and supportive throughout this project.

8 References

Alexeev V. A., Gorin V. D., Ivliev A. I., Kashkarov L. L., and Ustinova G. K. 2008. Recently Fallen Bukhara (CV3) and Kilabo (LL6) Chondrites: A Parallel Study of Luminescence, Tracks, and Cosmogenic Radionuclides. *Geochemistry International* 46:849–866.

Alwmark C., and Schmitz B. 2009. Relict silicate inclusions in extraterrestrial chromite and their use in the classification of fossil chondritic material. *Geochimica et Cosmochimica Acta* 73:1472-1486.

Alwmark C., Schmitz B., Holm S., Marone F., and Stampanoni M. 2011. A 3-D study of mineral inclusions in chromite from ordinary chondrites using synchrotron radiation X-ray tomographic microscopy—Method and applications. *Meteoritics & Planetary Science* 46:1071-1081.

Anders E., and Grevesse N. 1989. Abundances of the elements: Meteoritic and solar. *Geochimica et Cosmochimica Acta* 53:197-214.

Asplund M., Grevesse N. and Sauval A.J. 2005. The solar chemical composition. In *Cosmic abundances as records of stellar evolution and nucleosynthesis*, edited by Bash F.N. and Barnes T.G. San Francisco: ASP Conference Series. pp. 25-38.

Berezhko E.G., and Völk H.J. 2007. Spectrum of cosmic rays produced in supernova remnants. *The Astrophycical Journal* 661:175-178.

Bevan A.W.R, Bland P.A., and Jull J.T. 1998. Meteorite flux on the Nullarbor Region, Australia. In *Meteorites: Flux with Time and Impact Effects*, edited by Grady M., Hutchison R., McCall G.J.H. and Rothery D.A. London: Geological Society London Special Publications 140. pp. 59-73.

Bhattacharya S.K. Goswami J.N., and Lal D. 1973. Semiempirical Rates of Formation of Cosmic Ray Tracks in Spherical Objects Exposed in Space: Preatmospheric and Postatmospheric Depth Profiles. *Journal of Geophysical Research* 78:8356-8363.

Bradley J. P., Brownlee D. E., and Fraundorf P. 1984. Discovery of Nuclear Tracks in Interplanetary Dust. *Science* 226:1432-1434.

Bridges J.C., Schmitz B., Hutchison R., Greenwood R.C., Tassinari M., and Franchi I.A. 2007. Petrographic classification of mid-Ordovician fossil meteorites from Sweden. *Meteoritics & Planetary Science* 42: 1781-1789.

Brearley A.J., and Jones R.H. 1998. Chondritic Meteorites. In *Planetary Materials*, edited by Papike J.J. pp. 3.1-3.398.

Bull R.K., and Durrani S.A. 1976. Cosmic Ray Tracks in the Shalka Meteorite. *Earth and Planetray Science Letters* 32: 35-39.

Caffee M.W., Hohenberg C.M., Swindle T.D., and

Goswami J.N., 1987. Evidence in Meteorites for an Active Early Sun. *The Astrophysical Journal* 313: 31-35.

Castellina A., and Quispe Quispe A. 2009. Charged Cosmic Rays up to the knee region and beyond. *Proceedings, 3rd School on Cosmic Rays and Astrophysics. AIP Conference Proceedings* 1123:79-93.

Crozaz G., Haack U., Hair M., Maurette M., Walker R., and Woolum D. 1970. Nuclear track studies of ancient solar radiations and dynamic lunar surface processes. Proceedings, 3ed Apollo 11 Lunar Science Conference, pp. 2051-2080.

Crozaz G., Pellas P., Bourot-Denise M., de Chazal S.M., Fiéni C., Lundberg L.L., and Zinner E. 1989. Plutonium, uranium and rare earths in the phosphates of ordinary chondrites-the quest for a chronometer. *Earth and Planetary Science Letters* 93:157-169.

Fleischer R. L., Price P. B., and Walker R. M., 1965: Solid-State Track Detectors: Applications to Nuclear Science and Geophysics. *Annual Review of Nuclear Science* 15: 1-28.

Fleischer R.L., Price P.B. and Walker R.M. 1975. *Nuclear tracks in solids: principles and applications* Berkley: University of California Press. 605p.

Friedlander M.W. 2000. *A thin cosmic rain : particles from outer space*, 2nd ed. Cambridge: Harvard University Press. 241p.

Gleadow A.J.W., Duddy I.R., Green P.F., and Lovering J.F. 1986. Confined fission track lengths in apatite: a diagnostic tool for thermal history analysis. *Contributions to Mineralogy and Petrology* 94:405-415.

Grevesse N. and Sauval A.J. 1998. Standard Solar Composition. *Space Science Reviews* 85:161-174.

Grist A.M. 2004. Aspects of the thermal history of the eastern margin of Canada based on apatite fission track and (U/Th)/He thermochronology, Ph.D. thesis, Dalhousie University, Halifax, Nova Scotia, Canada.

Heck, P.R., Schmitz B., Baur H., Wieler R. 2008. Noble gases in fossil micrometeorites and meteorites from 470 Myr old sediments from southern Sweden, and new evidence for the L-chondrite parent body breakup event. *Meteoritics and Planetary Sciences* 43:517-528.

Holm S., Alwmark C., Alwarez W., and Schmitz B. 2011. Shock barometry of the Siljan impact structure, Sweden. *Meteoritics & Planetary Science* 46:1888-1909.

Hurford A.J., Platt J.P., and Carter A. 1999. Fission-track analysis of samples from the alboran sea basement. *Proceedings of the Ocean Drilling Program, Scientific Results* 161:295-300.

Huchison R. 2004. Meteorites: *A Petrologic, Chemical and Isotopic Synthesis.* Cambridge: Cambridge University Press. 506p.

James K. and Durrani S.A. 1986 The Effect Of Crystal Composition On Fission-Track Annealing and Closure Temperatures in Geological Minerals: Implications for the Cooling Rates of Terrestrial and Extraterrestrial Rocks. *Nuclear Tracks and Radiation Measurements* 11:277-282

Ketcham R.A., Donelick R.A., and Carlson W.D. 1999. Variability of apatite fission-track annealing kinetics: III. Extrapolation to geological time scales. *American Mineralogist* 84:1235- 1255.

Korochantseva E.V., Trieloff M., Lorenz C.A., Buykin A.I., Ivanova M.A, Schwarz W.H., Hopp J., and Jessberger E.K. 2007. L-chondrite asteroid breakup tied to Ordovician meteorite shower by multiple isochron 40Ar-39Ar dating. *Meteoritics & Planetary Science* 42:113–130.

Krishnaswami S., Lal D., Prabhu N., and Tamhane A. S. 1971.: Olivines: Revelation of Tracks of Charged Particles. *Science* 174:287-291.

Königshof P. 2003. Conodont deformation patterns and textural alteration in Paleozoic conodonts: examples from Germany and France. *Sencken bergiana lethaea* 83: 149-156.

Lal D. 1969. Recent advances in the study of fossil tracks in meteorites due to heavy nuclei of the cosmic radiation. *Space Science Reviews* 9:623 -650.

Lal D., Muralli A.V., Rajan R.S., Tamhane A.S., Lorin J.C., and Pellas P. 1968. Techniques for proper revelation and viewing of etch-tracks in meteor itic and terrestrial minerals. *Earth and Plane tary Science Letters* 5:111-119.

Letessier-Selvon A., and Stanev T. 2011. Ultrahigh energy cosmic rays. *Reviews of Modern Physics* 83:907-942.

Lindskog A. 2011. A Russian record of a Middle Ordovician meteorite shower: Extraterrestrial chromite in Volkhovian-Kundan (lower Darriwilian) strata at Lynna River, St. Petersburg region. Master thesis, Lund University, Lund, Sweden.

Love S.G., and Brownlee D.E. 1991. Heating and Thermal Transformation of Micrometeoroids Entering the Earth's Atmosphere. *Icarus* 89:26-43.

Marti K., and Lavielle B. 2009. History of the solar environment. In *Universal heliophysical processes*, edited by Gopalswamy N., and Webg D.F. Cambridge: Cambridge University Press. pp. 465-469.

Meier M.M.M., Schmitz B, Baur H., and Wieler R. 2010. Noble gases in individual L chondritic micrometeorites preserved in an Ordovician limestone. *Earth and Planetary Science Letters* 290:54-63.

Mellgren J.I.S., and Eriksson M.E. 2010. Untangling a Darriwilian (Middle Ordovician) palaeoecological event in Baltoscandia: conodont faunal changes across the 'Täljsten' interval.

Earth and Environmental Science Transactions of the Royal Society of Edinburgh 100: 353–370.

Metzler K. 2004 Formation of accretionary dust mant les in the solar nebula: Evidence from pre-irradiated olivines in CM chondrites. *Meteoritics & Planetary Science* 39:1307–1319.

Pellas P., and Storzer D. 1981. 244 Pu Fission Track Thermometry and its Application to Stony Meteorites. *Proceedings of the Royal Society of London. Series A, Mathematical and Physical Sciences* 374:253-270.

Perron, C. 1993. Cosmic ray-induced spallation recoil tracks in meteoritic phosphates: Simulation at the Cern synchrocyclotron. *Nuclear tracks and radiation measurements* 22:739-744.

Perron C. & Zanda B. 2005. Meteorites: samples of NEOs in laboratory. *Physique* 6: 345-360.

Peucker-Ehrenbrink B., and Ravizza G. 2000. The effects of sampling artifacts on cosmic dust flux estimates: A reevaluation of nonvolatile tracers (Os, Ir). *Geochimica et Cosmochimica Acta* 64: 1965-1970.

Price P.B., and Walker R.M. 1962a. Chemical Etching of Charged-Particle Tracks in Solids. *Journal of Applied Physics* 33: 3407-3412.

Price P.B., and Walker R.M. 1962b. Observations of Charged-Particle Tracks in Solids. *Journal of Applied Physics* 33:3400-3406.

Price P.B., Lal D., Tamhane A.S., and Perelygin V.P. 1973. Characteristics of tracks of ions of $14 \leq Z \leq 36$ in common rock silicates. *Earth and Planetary Science Letters* 19:377-395.

Ptuskin V., Zirakashvili V., and Seo E.S. 2010. Spectrum of Galactic Rays Accelerated in Supernova Remnants. *Astrophysical Journal* 718:31-36

Rabone J. A. L., Carter A., Hurford A. J. and de Lee uw N. H. 2008. Modelling the formation of fission tracks in apatite minerals using molecu lar dynamics simulations. *Physics and chemistry of minerals* 35:583-596

Ramdohr P. 1973.*The Opaque Minerals in Stony Meteorites*. Amsterdam: Elsevier. 245p.

Reiners P.W., and Branton M.T. 2006. Using Thermochronology to Understand Orogenic Erosion. *Annual Reviews in Earth and Planetary Sciences* 34:419-66.

Rogers N. 2007. *An Introduction to Our Dynamic Planet.* Cambridge: The University Press. 345p.

Schmitz B., Tassinari M., and Peucker-Ehrenbrink B. 2001. A rain of ordinary chondrites in the early Ordovician. *Earth and Planetary Science Letters* 194:1-15.

Schmitz B., Häggström T., and, Tassinari M. 2003. Sediment-dispersed extraterrestrial chromite traces a major asteroid disruption event. *Science* 300:961-964.

Schmitz B., and Häggström T. 2006. Extraterrestrial chromite in Middle Ordovician marine limestone at Kinnekulle, southern Sweden – Traces of a major asteroid breakup event. *Meteoritics & Planetary Science* 41:455-466.

Shaviv, N.J. 2002. Cosmic ray diffusion from the galactic spiral arms, iron meteorites, and a possible climatic connection? *Physical Review Letters* 89:1-4.

Shaviv N.J., and Veizer J. 2003. Celestial driver of Phanerozoic climate? *GSA Today* 13:4-10.

Söderlund U., and Johansson L. 2002. A simple way to extract baddeleyite (ZrO2). Geochemistry, Geophysics, and Geosystems 3:1014-1021.

Thorslund P., Wickman F.E., and Nyström J.O. 1984. The Ordovician chondrite from Brunflo, central Sweden, I. General description and primary minerals. *Lithos* 17:87-100.

Van Schmus W.R. and Wood J.A. 1967. A chemical-petological classification for the chondritic meteorites. *Geochimica et Cosmochimica Acta* 31:747-765.

Wagner G.A. 1968. Fission Track Dating of Apatites. *Earth and Planetary Science Letters* 4:411-415.

Young D.A. 1997. On the mechanism of the formation of latent tracks in dielectric solids. *Radiation Measurements* 27: 575-586.

Yuhas D.E., Walker R.M., Reeves H., Poupeau G., Pellas P., Lorin J.C., Chetrit G.C., Berdot J.L., Price P.B., Hutcheon I.D., Hart Jr. H.R., Fleischer R.L., Comstock G.M., Lal D., Goswami J.N., and Bhandari N. 1972. Track consortium report on rock 14310. *Proceedings, 3ed Lunar Science Conference*. pp.2941- 2947.

Tidigare skrifter i serien "Examensarbeten i Geologi vid Lunds Universitet":

249. Andersen, Christine, 2009: The mineral composition of the Burkland Cu-sulphide deposit at Zinkgruvan, Sweden – a supplementary study. (15 hskp)
250. Riebe, My, 2009: Spinel group minerals in carbonaceous and ordinary chondrites. (15 hskp)
251. Nilsson, Filip, 2009: Föroreningsspridning och geologi vid Filborna i Helsingborg. (30 hskp)
252. Peetz, Romina, 2009: A geochemical characterization of the lower part of the Miocene shield-building lavas on Gran Canaria. (45 hskp)
253. Åkesson, Maria, 2010: Mass movements as contamination carriers in surface water systems – Swedish experiences and risks.
254. Löfroth, Elin, 2010: A Greenland ice core perspective on the dating of the Late Bronze Age Santorini eruption. (45 hskp)
255. Ellingsgaard, Óluva, 2009: Formation Evaluation of Interlava Volcaniclastic Rocks from the Faroe Islands and the Faroe-Shetland Basin. (45 hskp)
256. Arvidsson, Kristina, 2010: Geophysical and hydrogeological survey in a part of the Nhandugue River valley, Gorongosa National Park, Mozambique. (45 hskp)
257. Gren, Johan, 2010: Osteo-histology of Mesozoic marine tetrapods – implications for longevity, growth strategies and growth rates. (15 hskp)
258. Syversen, Fredrikke, 2010: Late Jurassic deposits in the Troll field. (15 hskp)
259. Andersson, Pontus, 2010: Hydrogeological investigation for the PEGASUS project, southern Skåne, Sweden. (30 hskp)
260. Noor, Amir, 2010: Upper Ordovician through lowermost Silurian stratigraphy and facies of the Borenshult-1 core, Östergötland, Sweden. (45 hskp)
261. Lewerentz, Alexander, 2010: On the occurrence of baddeleyite in zircon in silica-saturated rocks. (15 hskp)
262. Eriksson, Magnus, 2010: The Ordovician Orthoceratite Limestone and the Blommiga Bladet hardground complex at Horns Udde, Öland. (15 hskp)
263. Lindskog, Anders, 2010: From red to grey and back again: A detailed study of the lower Kundan (Middle Ordovician) 'Täljsten' interval and its enclosing strata in Västergötland, Sweden. (15 hskp)
264. Rääf, Rebecka, 2010: Changes in beyrichiid ostracode faunas during the Late Silurian Lau Event on Gotland, Sweden. (30 hskp)
265. Petersson, Andreas, 2010: Zircon U-Pb, Hf and O isotope constraints on the growth versus recycling of continental crust in the Grenville orogen, Ohio, USA. (45 hskp)
266. Stenberg, Li, 2010: Geophysical and hydrogeological survey in a part of the Nhandugue River valley, Gorongosa National Park, Mozambique – Area 1 and 2. (45 hskp)
267. Andersen, Christine, 2010: Controls of seafloor depth on hydrothermal vent temperatures - prediction, observation & 2D finite element modeling. (45 hskp)
268. März, Nadine, 2010: When did the Kalahari craton form? Constraints from baddeleyite U-Pb geochronology and geo-chemistry of mafic intrusions in the Kaapvaal and Zimbabwe cratons. (45 hp)
269. Dyck, Brendan, 2010: Metamorphic rocks in a section across a Svecnorwegian eclogite-bearing deformation zone in Halland: characteristics and regional context. (15 hp)
270. McGimpsey, Ian, 2010: Petrology and lithogeochemistry of the host rocks to the Nautanen Cu-Au deposit, Gällivare area, northern Sweden. (45 hp)
271. Ulmius, Jan, 2010: Microspherules from the lowermost Ordovician in Scania, Sweden – affinity and taphonomy. (15 hp)
272. Andersson, Josefin, Hybertsen, Frida, 2010: Geologi i Helsingborgs kommun – en geoturistkarta med beskrivning. (15 hp)
273. Barth, Kilian, 2011: Late Weichselian glacial and geomorphological reconstruction of South-Western Scania, Sweden. (45 hp)
274. Mashramah, Yaser, 2011: Maturity of kerogen, petroleum generation and the application of fossils and organic matter for paleotemperature measurements. (45 hp)
275. Vang, Ina, 2011: Amphibolites, structures and metamorphism on Flekkerøy, south Norway. (45 hp)
276. Lindvall, Hanna, 2011: A multi-proxy study of a peat sequence on Nightingale

Island, South Atlantic. (45 hp)

277. Bjerg, Benjamin, 2011: Metodik för att förhindra metanemissioner från avfallsdeponier, tillämpad vid Albäcksdeponin, Trelleborg. (30 hp)
278. Pettersson, Hanna, 2011: El Hicha – en studie av saltstäppssediment. (15 hskp)
279. Dyck, Brendan, 2011: A key fold structure within a Sveconorwegian eclogite-bearing deformation zone in Halland, southwestern Sweden: geometry and tectonic implications. (45 hp)
280. Hansson, Anton, 2011: Torvstratigrafisk studie av en trädstamshorisont i Viss mosse, centrala Skåne kring 4 000 - 3 000 cal BP med avseende på klimat- och vattenståndsförändringar. (15 hp)
281. Åkesson, Christine, 2011: Vegetationsutvecklingen i nordvästra Europa under Eem och Weichsel, samt en fallstudie av en submorän, organisk avlagring i Bellinga stenbrott, Skåne. (15 hp)
282. Silveira, Eduardo M., 2011: First precise U-Pb ages of mafic dykes from the São Francisco Craton. (45 hp)
283. Holm, Johanna, 2011**:** Geofysisk utvärdering av grundvattenskydd mellan väg 11 och Vombs vattenverk. (15 hp)
284. Löfgren, Anneli, 2011: Undersökning av geofysiska metoders användbarhet vid kontroll av den omättade zonen i en infiltrationsdamm vid Vombverket. (15 hp)
285. Grenholm, Mikael, 2011: Petrology of Birimian granitoids in southern Ghana - petrography and petrogenesis. (15 hp)
286. Thorbergsson, Gunnlaugur, 2011: A sedimentological study on the formation of a hummocky moraine at Törnåkra in Småland, southern Sweden. (45 hp)
287. Lindskog, Anders, 2011: A Russian record of a Middle Ordovician meteorite shower: Extraterrestrial chromite in Volkhovian-Kundan (lower Darriwilian) strata at Lynna River, St. Petersburg region. (45 hp)
288. Gren, Johan, 2011: Dental histology of Cretaceous mosasaurs (Reptilia, Squamata): incremental growth lines in dentine and implications for tooth replacement. (45 hp)
289. Cederberg, Julia, 2011: U-Pb baddelyit dateringar av basiska gångar längs Romeleåsen i Skåne och deras påverkan av plastisk deformation i Protoginzonen (15 hp)
290. Ning, Wenxing, 2011: Testing the hypothesis of a link between Earth's magnetic field and climate change: a case study from southern Sweden focusing on the 1st millennium BC. (45 hp)
291. Holm Östergaard, Sören, 2011: Hydrogeology and groundwater regime of the Stanford Aquifer, South Africa. (45 hp)
292. Tebi, Magnus Asiboh, 2011: Metamorphosed and partially molten hydrothermal alteration zones of the Akulleq glacier area, Paamiut gold province, South-West Greenland. (45 hp)
293. Lewerentz, Alexander, 2011: Experimental zircon alteration and baddeleyite formation in silica saturated systems: implications for dating hydrothermal events. (45 hp)
294. Flodhammar, Ingrid, 2011: Lövestads åsar: En isälvsavlagring bildad vid inlandsisens kant i Weichsels slutskede. (15 hp)
295. Liu, Tianzhuo, 2012: Exploring long-term trends in hypoxia (oxygen depletion) in Western Gotland Basin, the Baltic Sea. (45 hp)
296. Samer, Bou Daher, 2012: Lithofacies analysis and heterogeneity study of the subsurface Rhaetian–Pliensbachian sequence in SW Skåne and Denmark. (45 hp)
297. Riebe, My, 2012: Cosmic ray tracks in chondritic material with focus on silicate mineral inclusions in chromite. (45 hp)

LUNDS UNIVERSITET

Geologiska institutionen
Lunds universitet
Sölvegatan 12, 223 62 Lund